The epidermal polarity protein Par3 is a non–cell autonomous suppressor of malignant melanoma

Melina Mescher,[1,3]* Peter Jeong,[1,3]* Sina K. Knapp,[1,3] Matthias Rübsam,[1,2] Michael Saynisch,[1] Marina Kranen,[1,3] Jennifer Landsberg,[4,5] Max Schlaak,[2] Cornelia Mauch,[2] Thomas Tüting,[5,6] Carien M. Niessen,[1,2,3] and Sandra Iden[1,3]

[1]Cologne Excellence Cluster on Cellular Stress Responses in Aging-Associated Diseases, [2]Department of Dermatology, and [3]Center for Molecular Medicine Cologne, University of Cologne, 50923 Köln, Germany
[4]Laboratory of Immunodermatology, Department of Dermatology, Venereology, and Allergology, University Hospital Essen, and German Cancer Consortium, Partner Site Essen/Düsseldorf, West German Cancer Center, University of Duisburg-Essen, 45122 Essen, Germany
[5]Laboratory of Experimental Dermatology, Department of Dermatology and Allergy, University of Bonn, 53115 Bonn, Germany
[6]Department of Dermatology, University Hospital Magdeburg, 39120 Magdeburg, Germany

Melanoma, an aggressive skin malignancy with increasing lifetime risk, originates from melanocytes (MCs) that are in close contact with surrounding epidermal keratinocytes (KCs). How the epidermal microenvironment controls melanomagenesis remains poorly understood. In this study, we identify an unexpected non–cell autonomous role of epidermal polarity proteins, molecular determinants of cytoarchitecture, in malignant melanoma. Epidermal Par3 inactivation in mice promotes MC dedifferentiation, motility, and hyperplasia and, in an autochthonous melanoma model, results in increased tumor formation and lung metastasis. KC-specific Par3 loss up-regulates surface P-cadherin that is essential to promote MC proliferation and phenotypic switch toward dedifferentiation. In agreement, low epidermal PAR3 and high P-cadherin expression correlate with human melanoma progression, whereas elevated P-cadherin levels are associated with reduced survival of melanoma patients, implying that this mechanism also drives human disease. Collectively, our data show that reduced KC Par3 function fosters a permissive P-cadherin–dependent niche for MC transformation, invasion, and metastasis. This reveals a previously unrecognized extrinsic tumor-suppressive mechanism, whereby epithelial polarity proteins dictate the cytoarchitecture and fate of other tissue-resident cells to suppress their malignant outgrowth.

INTRODUCTION

Malignant melanoma is one of the most aggressive types of cancer, with an increasing incidence and early and frequent metastasis to distant organs causing high lethality (Schadendorf et al., 2015). Melanoma development is considered a stepwise process. Clones of hyperproliferative melanocytes (MCs) typically undergo cellular senescence, forming benign nevi (Mooi and Peeper, 2006; Gray-Schopfer et al., 2007). However, different mutations, e.g., within the *INK4A/ARF* locus, enable cells to overcome senescence and to superficially spread within the epidermis (radial growth phase). These cells can then acquire the ability to invade into the underlying dermis (vertical growth phase) and subsequently metastasize.

Advances in the understanding of melanoma cell biology and immune regulation have led to the development of new targeted drugs, e.g., mutant BRAF or MEK inhibitors, that can prolong overall survival in patients with metastatic disease. In addition, PD-1/PD-L1 or CTLA4-directed immune checkpoint blockade that promotes antitumor T cell activation in the microenvironment showed remarkable treatment response (Schadendorf et al., 2015). Despite the recent success of immunotherapy and targeted therapy for melanoma patients, intrinsic and acquired resistance mechanisms determine the efficacy of these therapeutic approaches. Thus, new molecular targets are needed to overcome therapy resistance and to achieve long-term clinical responses.

Although the relevance of tumor–immune cell interactions to melanoma is established, it is less clear how other cell types in the microenvironment contribute to melanomagenesis. MCs are of neuroectodermal origin and are in intimate contact with keratinocytes (KCs), the main cell type of the skin epidermis. A single MC is in contact with ∼36 KCs (Fitzpatrick and Breathnach, 1963), providing them with melanin pigment that protects the skin against UV-induced damage (Van Den Bossche et al., 2006). Although

*M. Mescher and P. Jeong contributed equally to this paper.

Correspondence to Sandra Iden: sandra.iden@uk-koeln.de

Abbreviations used: CHO, Chinese hamster ovary; DMBA, 7,12-dimethylbenz[a] anthracene; EGFP, enhanced GFP; ERK, extracellular signal–regulated kinase; H&E, hematoxylin and eosin; HC, high calcium; HGF, hepatocyte growth factor; KC, keratinocyte; LC, low calcium; MC, melanocyte; PCNA, proliferating cell nuclear antigen; PFA, paraformaldehyde; TPA, 12-*O*-tetradecanoylphorbol-13-acetate.

The Rockefeller University Press $30.00
J. Exp. Med. 2017 Vol. 214 No. 2 339–358
https://doi.org/10.1084/jem.20160596

KCs have been reported to secrete soluble factors mediating MC growth, motility, and differentiation (Scott et al., 2007; Fukunaga-Kalabis et al., 2008; Bald et al., 2014; Coleman et al., 2015), the relevance of direct, physical KC–MC interaction for MC physiology and pathogenesis is less clear. KC–MC adhesions involve E-cadherin (Tang et al., 1994), which is thought to be essential to control MC growth (Haass and Herlyn, 2005), as E-cadherin loss is common during melanoma progression (Miller and Mihm, 2006). P-cadherin has also been reported to modulate homeostatic MC functions (Samuelov et al., 2012, 2013). During mouse development, melanoblasts migrate through the dermis, pass the dermal–epidermal junction around birth, populate the neonatal epidermis, and then mostly migrate into the developing hair follicles. In the bulge, MC stem cells reside throughout adulthood and are periodically coactivated with the hair follicle cycle and neighboring hair follicle stem cells (Slominski and Paus, 1993; Nishimura et al., 2002). Soluble factors released by adjacent bulge and bulb epithelial cells contribute to MC stem cell maintenance and activation, including TGFβ, Wnt, KIT ligand, and endothelin 2 (Botchkareva et al., 2001; Peters et al., 2002; Rabbani et al., 2011; Tanimura et al., 2011; Chang et al., 2013), highlighting that cellular cross talk is an important factor in MC homeostasis.

Despite the importance of KC–MC interactions for the epidermal melanin unit, the molecular basis of this communication and its relevance for melanomagenesis is poorly understood. MCs undergo striking morphological changes when homing to their epidermal niche, differentiating into melanin-producing dendritic MCs, and in the course of oncogenic transformation when they undergo hyperproliferation and dendritic shortening (Haass and Herlyn, 2005). Profound and dynamic changes in adhesion, cell polarity, and architecture of tumor cells are hallmarks of cancer and implicated in tumor growth, invasion, and metastasis (Hanahan and Weinberg, 2000). Conserved polarity proteins regulate a wide range of cell behaviors including neuronal differentiation, directed cell migration, apicobasal polarity, oriented cell divisions, and directed vesicular transport (Iden and Collard, 2008; Macara and Mili, 2008; St Johnston and Ahringer, 2010; Niessen et al., 2012). Polarity proteins couple the control of cell shape to crucial signaling pathways regulating cell growth and survival, metabolism, fate, and differentiation. The Par3–atypical protein kinase C (aPKC)–Par6 polarity complex has emerged as a key regulatory module of cellular asymmetry and is crucial for embryonic development (Suzuki and Ohno, 2006). Importantly, altered polarity protein expression has been observed in a range of human cancers (Huang and Muthuswamy, 2010; Murray et al., 2011). Recent studies using animal models with impaired polarity protein function revealed that tumor-intrinsic polarity signaling controls formation and progression of epithelial cancers (Gödde et al., 2014; Mescher and Iden, 2015). Our previous work identified Par3 as an important integrator of oncogenic Ras- and aPKC-mediated signaling and revealed tumor type–dependent prooncogenic and tumor-suppressive functions of Par3 in epidermal cancers (Iden et al., 2012). Despite this emerging cell-autonomous role of polarity proteins in cancer, it is largely unknown how the cytoarchitecture and polarity of the environment control tumor initiation and progression.

Here, we addressed the role of Par3 in the epithelial environment of melanoma and the control of KC–MC cross talk as a potential rheostat of MC transformation and malignancy.

RESULTS

Epidermal Par3 suppresses melanoma formation and metastasis in vivo

In chemical 7,12-dimethylbenz[a]anthracene (DMBA)/12-*O*-tetradecanoylphorbol-13-acetate (TPA) skin carcinogenesis experiments, we observed that mice with epidermal loss of Par3 (*K14Cre;Par3*$^{fl/fl}$; hereafter *Par3*^{eKO}) surprisingly showed increased melanocytic hyperplasia and incidence of melanoma (Fig. 1 A). As Par3 deletion was restricted to the keratin 14 (K14)–derived lineage and not occurring in MCs, which was also verified by Cre reporter analyses (Fig. 1 B), this implied that KC polarity proteins impinge on MC fate. To test this more rigorously, we crossed *Par3*^{eKO} mice to *hepatocyte growth factor (HGF);Cdk4*^{R24C} mice, a model for autochthonous malignant melanoma closely resembling human pathology (Fig. 1 C; Tormo et al., 2006). In this immunocompetent model, HGF expression retains interfollicular MCs (Takayama et al., 1997), mimicking MC localization in human skin, and mediates deregulated receptor tyrosine kinase signaling. An additional oncogenic *Cdk4*^{R24C} germline mutation impairs p16/Ink4a-dependent cell cycle regulation (Sotillo et al., 2001; Gray-Schopfer et al., 2006), a crucial tumor-suppressive axis that is defective in the vast majority of human melanoma (Young et al., 2014). *HGF;Cdk4*^{R24C} mice are prone to spontaneous melanoma, and genotoxic insults such as UV light or exposure to carcinogens like DMBA further accelerate and synchronize HGF;Cdk4^{R24C}-driven melanomagenesis (Gaffal et al., 2011; Landsberg et al., 2012). Intriguingly, combining this genetic melanoma model with Par3 loss in the epidermal environment revealed significantly increased melanoma multiplicity as compared with control littermates (Fig. 1, C and D), while Par3 expression was retained within the melanoma, further confirming that the K14-driven Cre recombinase used in this study is not active in MCs (Fig. 1 E). Primary melanoma invaded the dermis and showed tumor-associated angiogenesis (Fig. 1 F). Importantly, epidermal Par3 loss also promoted distant metastasis as the lungs of *Par3*^{eKO};*HGF*$^{+}$;*Cdk4*$^{R24C/R24C}$ mice exhibited increased incidence (57.1 vs. 16.7% in Ctrl;*HGF*$^{+}$;*Cdk4*$^{R24C/R24C}$) and number (Fig. 1, G and H) of pigmented metastatic lesions positive for the MC marker TRP2 (Fig. 1 I) and negative for F4/80 (not depicted), discriminating them from melanophages. Thus, these data demonstrate a hitherto unknown in vivo role for a polarity protein in non–cell autonomous suppression of cancer formation and progression.

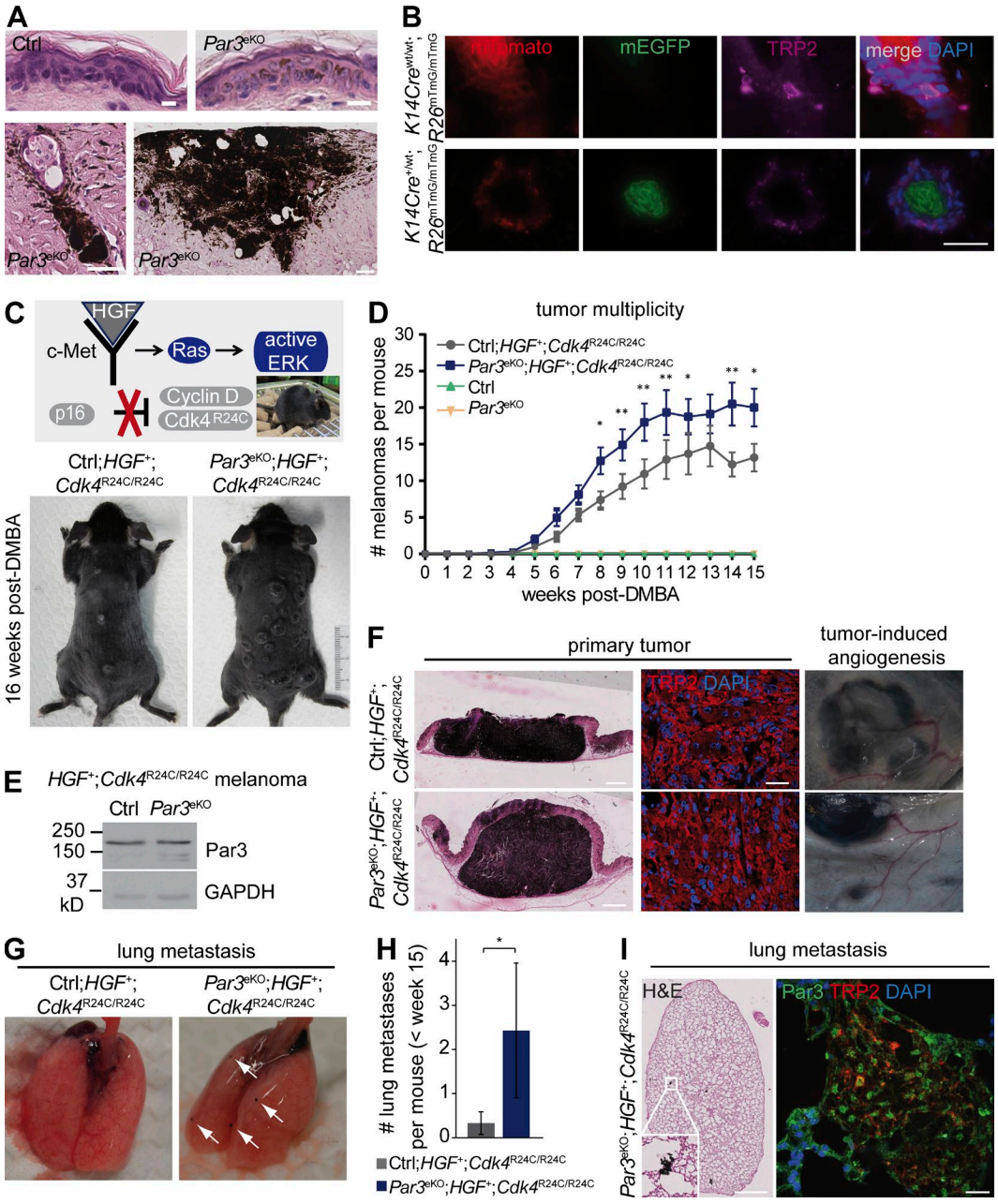

Figure 1. **Epidermal Par3 deletion results in elevated melanoma multiplicity and lung metastasis.** (A) Epidermis of DMBA/TPA-treated control (ctrl) and *Par3*^{eKO} mice, showing MC hyperplasia and melanoma in DMBA/TPA-treated *Par3*^{eKO} mice. H&E staining of back skin cross sections is shown. Bars: (top) 10 µm; (bottom left) 50 µm; (bottom right)100 µm. Data are representative of one skin tumor experiment with control (n = 25) and Par3^{eKO} (n = 27) mice. (B) Skin cross sections of mTmG dual-fluorescence reporter mice with and without K14Cre allele and simultaneous immunostaining for the MC marker TRP2. Note that K14Cre-mediated recombination as evident by switch from membranous red (mTomato) to green (EGFP) fluorescence does not occur in MCs. Bar, 25 µm. Data are represented from two independent experiments. n = 3 mice per group. (C) *HGF;Cdk4*^{R24C} mice: an autochthonous mouse melanoma model for spontaneous melanoma. (Top) Single topical DMBA treatment (or single UV exposure) serves to accelerate and synchronize melanoma formation. (Bottom) Representative photographs of control and *Par3*^{eKO} mice crossed to the *HGF;Cdk4*^{R24C} melanoma model (Ctrl;*HGF*$^{+}$;*Cdk4*$^{R24C/R24C}$ and *Par3*^{eKO};*HGF*$^{+}$;*Cdk4*$^{R24C/R24C}$) 16 wk after DMBA. (D) Tumor multiplicity in the melanoma model shown in C. Pooled data are depicted as mean ± SEM, with in total n (Ctrl;*HGF*$^{+}$;*Cdk4*$^{R24C/R24C}$) = 18 mice, n (*Par3*^{eKO}; *HGF*$^{+}$;*Cdk4*$^{R24C/R24C}$) = 22 mice, n (control) = 5 mice, and n (*Par3*^{eKO}) = 11 mice at the start of the experiment. P-values weeks 8–15 (left to right): *, P = 0.01242; **, P = 0.00931; **, P = 0.00125; **, P = 0.00456; *, P = 0.03295; NS, 0.07363; **, P = 0.00142; *, P = 0.01482; Ctrl;*HGF*$^{+}$;*Cdk4*$^{R24C/R24C}$ vs. *Par3*^{eKO};*HGF*$^{+}$;*Cdk4*$^{R24C/R24C}$; multiple Student's t tests. (E) Par3 and GAPDH immunoblots of protein extracts isolated from primary melanoma that developed in Ctrl;*HGF*$^{+}$;*Cdk4*$^{R24C/R24C}$ and *Par3*^{eKO};*HGF*$^{+}$;*Cdk4*$^{R24C/R24C}$ mice, demonstrating robust Par3 expression in melanoma that is unaffected by K14Cre-mediated recombination. Data are representative of three independent experiments. n = 3 biological replicates per group.

Par3 in KCs counteracts MC proliferation and survival through modulation of direct cell–cell contacts

To examine how Par3 loss in the epithelial environment promotes melanoma, we studied proliferation of primary tumors that developed in the HGF;Cdk4 melanoma model. These analyses revealed an increased proliferative index, with an elevated number of proliferating cell nuclear antigen (PCNA)^{high} melanoma cells in *Par3^{eKO};HGF^{+};Cdk4$^{R24C/R24C}$* mice (Fig. 2, A and B), in agreement with the higher tumor multiplicity. Moreover, melanomas in these mice displayed significantly increased extracellular signal–regulated kinase (ERK) and Akt activity (Fig. 2, C and D), indicating that Par3 deficiency in the epidermis stimulates growth and survival signaling in mouse melanoma. To assess whether Par3 already regulates MC behavior under nontumorigenic conditions, we examined epidermis and hair follicles of *Par3^{eKO}* mice at different ages for the presence of MCs. Following the route of MC homing, interfollicular MCs were analyzed in newborn epidermis, whereas hair follicle–localized MCs were studied in neonatal, young, and old adult mice. Immunohistochemical analysis revealed an increase in TRP2-positive MC number in the back skin of *Par3^{eKO}* mice compared with controls at all stages examined (Fig. 2, E–H). To assess whether epidermal Par3-mediated regulation of MC numbers depended on direct KC–MC interaction or was based on secreted factors, we performed different co-culture assays using primary mouse wild-type MCs and control or *Par3^{KO}* KCs. This revealed that loss of Par3 in KCs significantly expanded the number of MCs when compared with control cultures, but only when these two cell types were in direct contact and in the presence of 1.8 mM Ca^{2+} (high calcium [HC]; Fig. 2, I and J), whereas indirect co-cultures (Fig. 2 K) or direct co-cultures at low calcium (LC) conditions (50 µM Ca^{2+}; Fig. 2, I and J) did not affect MC number. MC expansion was mainly driven by a combination of increased proliferation and decreased apoptosis of MCs, as indicated by increased BrdU incorporation and reduced cleaved caspase3 immunoreactivity, respectively (Fig. 2, L and M). Together, in line with our in vivo observation of deregulated normal and transformed MCs when the extrinsic polarity machinery was disturbed, these data show that the loss of Par3 in KCs elicits increased MC proliferation and survival through direct and calcium-dependent KC–MC interactions.

Epidermal Par3 controls MC morphology and motility

In addition to increased growth and survival, we also noted significant changes of MC shape when co-cultured with *Par3^{KO}* KCs (Fig. 3 A). As Par3 has a well established role in the intrinsic regulation of cytoarchitecture, we assessed whether Par3 could affect cell shape in a non–cell autonomous manner. Phase-contrast and immunohistochemistry analyses revealed that MCs exposed to control KCs displayed long and thin dendrites and overall neuronal-like morphology, whereas they exhibited a flattening of the cell body and significantly shortened dendrites when exposed to *Par3^{KO}* KCs (Fig. 3, A–C), suggesting MC dedifferentiation. Similarly, in the skin of *Par3^{eKO}* mice, MCs displayed a more stubby dendritic morphology with dendritic shortening and more spread cell body area (Fig. 3, D and E). Time-lapse microscopy of co-cultures demonstrated larger contact areas of MCs with surrounding *Par3^{KO}* KCs and concomitant dendritic shortening. Strikingly, however, this increased interaction did not reflect more static intercellular adhesion; instead, MCs showed remarkably enhanced motility with continuous crawling in between *Par3^{KO}* KCs and frequent exchange of neighboring KCs. This was in stark contrast to control cultures where MCs connected to KCs largely via their dendritic tips, with little net movement of the whole cell (Videos 1 and 2). Automated morphometric analysis of TRP2-immunostained MCs confirmed these morphological changes, as indicated by decreased mean MC compactness when exposed to *Par3^{KO}* KCs (Fig. 3 F). To further assess the consequence of Par3 deficiency in KCs on MC shape and overall motility, we performed live-cell imaging of co-cultured MCs expressing fluorescent membrane-targeted Tomato (mT/mG; Muzumdar et al., 2007). Analysis of MC perimeters and tracking of individual MCs in co-cultures using Quimp11b software (Tyson et al., 2014) revealed that, despite more flattened and less dendritic morphology, loss of Par3 in KCs led to increased MC protrusion dynamics, with frequent formation and repositioning of cellular protrusions (Fig. 3 G). Notably, this coincided with increased total distance traveled and mean speed of MCs contacting Par3-deficient KCs compared with controls (Fig. 3 H). Although it remains formally possible that the observed increased lung metastasis in *Par3^{eKO};HGF^{+};Cdk4$^{R24C/R24C}$* mice was in part caused by an increased primary tumor load or altered angiogenesis, these independent single-cell analyses enabled us to uncouple MC number and motility. Together, the KC–MC co-culture experiments demonstrated that epidermal Par3 is

(F) H&E staining of primary melanoma in control and *Par3^{eKO}* melanoma mice. TRP2 immunohistochemistry of primary melanoma and macroscopically visible vascularization close to melanoma formed in these mice are shown. Bars: (left) 1 mm; (middle) 60 µm. Data are representative of at least three independent experiments (TRP-2 immunohistochemistry) or analyses of in total *n* (Ctrl;*HGF^{+};Cdk4$^{R24C/R24C}$*) = 18 mice and *n* (*Par3^{eKO}; HGF^{+};Cdk4$^{R24C/R24C}$*) = 22 mice (H&E and tumor vascularization). (G) Lung metastasis in Ctrl;*HGF^{+};Cdk4$^{R24C/R24C}$* and *Par3^{eKO};HGF^{+};Cdk4$^{R24C/R24C}$* melanoma mice. Arrows indicate macroscopically visible metastases. (H) Quantification of macrometastases per lung in Ctrl;*HGF^{+};Cdk4$^{R24C/R24C}$* (*n* = 12 mice) and *Par3^{eKO};HGF^{+};Cdk4$^{R24C/R24C}$* (*n* = 7 mice) during melanomagenesis <15 wk after DMBA. The mean includes all mice analyzed irrespective of metastasis status. Incidence of lung metastasis: Ctrl;*HGF^{+};Cdk4$^{R24C/R24C}$*, 16.7%; *Par3^{eKO};HGF^{+};Cdk4$^{R24C/R24C}$*, 57.1%. Pooled data are depicted as mean ± SEM. *, P = 0.0436; Mann Whitney *U* test. (I) H&E (left) and TRP2 (right) immunostaining of melanoma metastases in lung. Bars: (H&E)100 µm; (immunofluorescence) 20 µm. Data are representative of two independent experiments. *n* = 3 biological replicates.

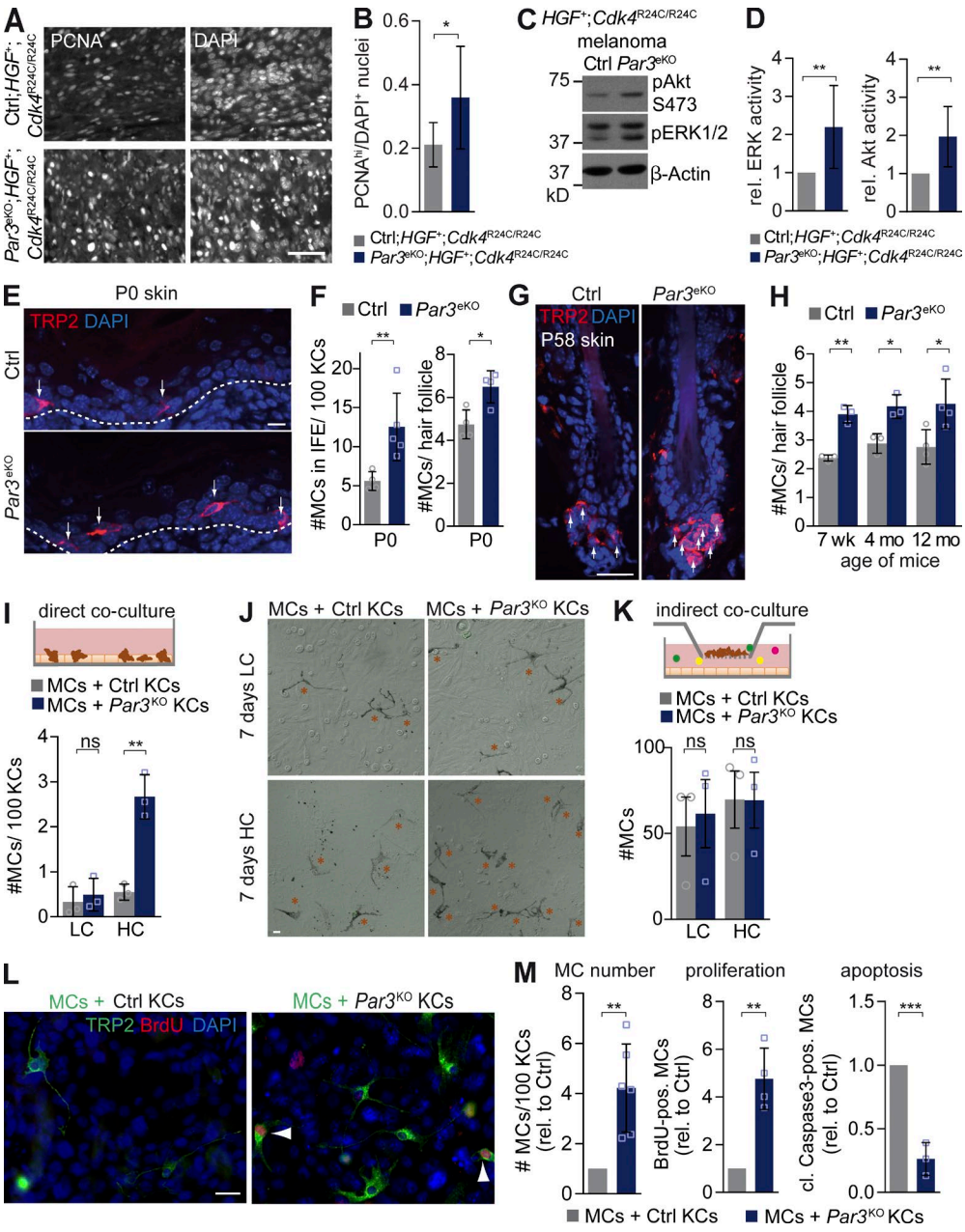

Figure 2. **Loss of epidermal Par3 promotes MC proliferation and survival through direct KC–MC contacts.** (A) PCNA immunostaining of primary melanoma formed in Ctrl;HGF^{+};$Cdk4^{R24C/R24C}$ and $Par3^{eKO}$;HGF^{+};$Cdk4^{R24C/R24C}$ mice. DAPI served as a nuclear counterstain. Bar, 25 µm. (B) Quantification of A. Relative proliferative index, determined as fraction of DAPI nuclei with high PCNA expression, is shown. Data are mean ± SD. *n* (control) = 5; *n* (KO) = 8. *, P = 0.0453; unpaired Student's *t* test with Welch's correction. Data are pooled from three independent experiments. (C) Phospho-ERK, phospho-Akt, and β-actin immunoblots of protein extracts isolated from primary melanoma that developed in Ctrl;HGF^{+};$Cdk4^{R24C/R24C}$ and $Par3^{eKO}$;HGF^{+};$Cdk4^{R24C/R24C}$ mice. (D) Quantification of C. Immunosignals of phosphorylated ERK and Akt were first normalized to β-actin (loading control) and then normalized to values of control tumors. Data are mean ± SD. pERK: *n* = 8 tumors per group; **, P = 0.0076. pAKT: *n* = 7 tumors per group; **, P = 0.00695. Student's *t* test was used. Data are pooled from three independent experiments, with each tumor originating from a different mouse. (E) TRP2 immunostaining for MCs in neonatal (P0) back skin cross sections of control and $Par3^{eKO}$ mice. Arrows mark MCs, and dashed lines underline the MC-containing basal epidermal layer. (F) Quantification of MC number in interfollicular epidermis of control (*n* = 4 independent biological replicates) and $Par3^{eKO}$ (*n* = 5 biological replicates). Data are mean ± SD. P0 back skin: **, P = 0.0076; Student's *t* test. Hair follicles: *n* = 4 biological replicates per group; *, P = 0.0129; Student's *t* test. (G) TRP2 immunostaining of P58 back skin cross sections of control and $Par3^{eKO}$ mice. Arrows indicate MCs. Data are representative of three independent experiments. (H) Quantification of MC number per hair follicle of control and $Par3^{eKO}$ back skins of adult mice of different age. Data are pooled from independent experiments and depicted as mean ± SD. 7 wk: *n* = 3 biological replicates per group; **, P = 0.0012. 4 mo: *n* = 3 biological replicates per group; *, P = 0.0139. 12 mo: *n* = 4 biological replicates per group; *, P = 0.0291. Student's *t* test was used. (I) Scheme of direct co-cultures (top) and quantification of direct co-cultures

a crucial regulator of MC morphology that counteracts MC migration and protrusive activity, both processes that can facilitate increased melanoma metastasis.

Loss of epidermal Par3 results in elevated P-cadherin localization at heterologous KC–MC contacts

The direct KC–MC co-cultures revealed that Par3 deficiency leads to increased MC proliferation, survival, and migration and dendritic shortening at high extracellular calcium that not only promotes differentiation of KCs, but also induces Ca^{2+}-dependent adhesion. As the co-cultures required direct contact, we therefore hypothesized that calcium-dependent adhesion molecules were crucial for the abnormal *Par3*^{KO} KC–MC cross talk. In line with previous studies, we were able to detect E- and P-cadherin expression in both KCs and MCs (Fig. 4, G and H). E-cadherin has previously been implicated in mediating KC–MC contacts in humans (Tang et al., 1994), and mice with MC-specific E-cadherin deletion exhibit partial MC loss after stress, mimicking clinical vitiligo (Wagner et al., 2015). However, we could only detect modest E-cadherin localization at heterologous junctions (not depicted). Then, we examined P-cadherin, as this classical cadherin is also expressed in the epidermis, and found a strong enrichment of P-cadherin at sites of KC–MC adhesion but not in homologous MC–MC contacts (Fig. 4, A and B). Notably, P-cadherin localization to heterologous junctions was reinforced between MCs and *Par3*^{KO} KCs as compared with control KCs (Fig. 4 B). Moreover, P-cadherin was also localized at sites of contacts between KCs and MCs in vivo (Fig. 4, C and D), indicating that P-cadherin mediates heterologous contacts between two resident skin cells. In addition, we noted an inverse correlation of Par3 and P-cadherin in the skin of wild-type mice: in areas of high P-cadherin immunoreactivity such as the hair matrix and basal epidermal layer (Müller-Röver et al., 1999; Tinkle et al., 2008), Par3 levels were reduced, whereas in P-cadherin low-expressing compartments, such as the suprabasal epidermis, Par3 immunoreactivity was high (Fig. 4 C). Therefore, we examined the consequence of *Par3* inactivation on P-cadherin localization in vivo. Strikingly, P-cadherin–positive clusters were bigger in *Par3*^{eKO} epidermis, with frequent localization of MCs to these compartments. Similarly, more MCs contacted dense P-cadherin^{high} clusters in developing *Par3*^{eKO} hair follicles (Fig. 4, D and E). Hence, we assessed whether overall P-cadherin expression was affected by loss of Par3. Whereas we could not detect changes in P-cadherin RNA expression (Fig. 4 F), surface biotinylation experiments of control or *Par3*^{KO};*HGF*$^{+}$;*Cdk4*$^{R24C/R24C}$ KC–MC co-cultures demonstrated significantly increased cell-surface levels of P-cadherin, but not E-cadherin, in Par3-deficient KCs as compared with controls (Fig. 4, I and J). Importantly, pulse-chase experiments also unraveled significantly higher P-cadherin protein stability upon Par3 inactivation (Fig. 4, K and L). Thus, loss of Par3 in KCs decreases P-cadherin turnover and selectively elevates surface P-cadherin on KCs, which through homotypic cadherin transinteraction may subsequently stabilize P-cadherin on co-cultured MCs.

P-cadherin mediates MC hyperplasia and shape changes upon Par3 loss

To directly test whether increased P-cadherin was responsible for the morphological and mitogenic changes of MCs upon loss of epidermal Par3, we inhibited P-cadherin–mediated adhesion using a function-blocking antibody (PCD-1; Nose and Takeichi, 1986) in KC–MC co-cultures. Strikingly, whereas an E-cadherin function–blocking antibody that delayed calcium-induced cell–cell contact formation between KCs (not depicted) had no impact on the morphology of MCs in *Par3*^{KO} KC co-culture (Fig. 5 A), P-cadherin block resulted in a complete rescue of dendritic MC morphology (Fig. 5, A and B). Similarly, siRNA-mediated P-cadherin down-regulation in *Par3*^{KO} KCs reversed MC dendritic length and prevented MC expansion (Fig. 5, C–E), showing that P-cadherin was necessary for MC changes in a Par3-deficient microenvironment.

To test whether P-cadherin up-regulation in vivo is sufficient for MC expansion and dendritic shortening, we made use of mice with epidermal deletion of E-cadherin resulting in compensatory up-regulation of P-cadherin in the basal epidermal layer (Tinkle et al., 2004; Tunggal et al., 2005). In line with our hypothesis that KC-expressed P-cadherin promotes MC expansion, *E-cadherin*^{KO} epidermis (Tunggal et al., 2005) displayed increased MC numbers (Fig. 6, A and B), thus mimicking *Par3*^{eKO} skin. Moreover, MCs co-cultured with *E-cadherin*^{KO} KCs, characterized by increased P-cadherin expression (Fig. 6 C), recapitulated MC expansion and decreased dendritic length (Fig. 6, D and E) as observed in co-culture with *Par3*^{KO} KCs. Importantly, these MC

(bottom), cultivated 7 d in LC and HC medium (five images/condition) The graph shows pooled data from independent experiments depicted as mean ± SD. *n* = 3 biological replicates per group. **, P = 0.0022; Student's *t* test). (J) Phase-contrast micrography of direct co-cultures. Orange asterisks mark MCs. (K) Scheme and quantification of MC number per image in indirect co-culture with control and *Par3*^{KO} KCs (greater than nine images/condition) The graph show pooled data from independent experiments as mean ± SEM. *n* = 3 biological replicates per group. LC: ns, P = 0.79. HC: ns, P = 0.99. Student's *t* test was used. Subconfluent MCs cultured on a permeable filter support were indirectly co-cultured with control or Par3-deficient KC cultures. (L) BrdU and TRP2 immunostaining of direct co-cultures. Arrowheads mark BrdU-positive MCs. Data are representative of three independent experiments. (M) Quantification of MC number directly co-cultured with control or *Par3*^{KO} KCs for 10 d at HC (left) and percentage of MCs positive for BrdU (middle) or cleaved caspase3 (right; >10 images per condition). The graphs show pooled data from independent experiments depicted as mean ± SD. MC: *n* = 6 biological replicates per group; **, P = 0.0012. Proliferation: *n* = 4 biological replicates per group; **, P = 0.0011. Apoptosis: *n* = 3 biological replicates per group; ***, P = 0.0006. Student's *t* test was used. cl., cleaved; Ctrl, control; IFE, interfollicular epidermis, pos., positive; rel., relative. Bars: (E and L) 10 µm; (G and J) 20 µm.

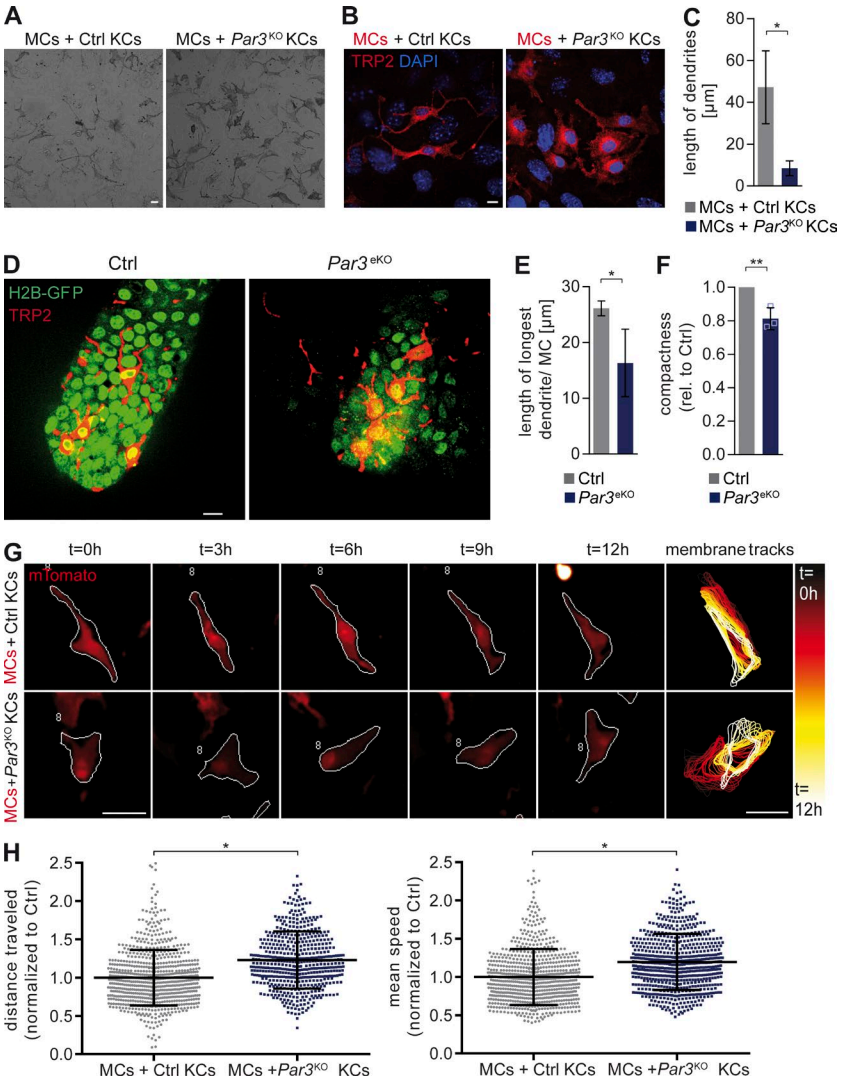

Figure 3. **MC morphology, protrusion dynamics, and migration is regulated by epidermal Par3.** (A) Phase-contrast micrography and live-cell imaging of mouse KC–MC co-cultures (stills of Videos 1 and 2; 4 d co-culture; HC medium). Data are representative of two independent experiments. (B) TRP2 immunostaining of MC co-cultures with control or *Par3*^{KO} KCs. Data are representative of three independent experiments. (C) Quantification of B. MC dendritic length in direct co-cultures 7 d in HC medium (>20 images/condition) is shown. Data are pooled from independent experiments represented as mean ± SD. *n* = 3 biological replicates per group. *, P = 0.0196; Student's *t* test. (D) TRP2 immunostaining of tail whole mounts of control and *Par3*^{eKO};H2B-GFP^{+} mice (age: P58). (E) Quantification of in vivo MC morphology in tail whole mounts (>10 hair follicles per mouse). Data are pooled from independent experiments and are depicted as mean ± SD. *n* = 5 biological replicates per group. *, P = 0.0208; unequal variances Student's *t* test with Welch's correction. (F) Automated, unbiased quantification of MC compactness using CellProfiler (>20 images/condition). A low value for compactness reflects a MC shape that is closer to a perfect circle than higher values for compactness. Data are pooled from independent experiments and depicted as mean ± SD. *n* = 3 biological replicates per group. **, P = 0.0078; Student's *t* test. (G) Live-cell imaging of membraneTomato (*mT/mG*)-expressing control MCs co-cultured with control or *Par3*^{KO} KCs (4-d co-culture; HC medium). From left to right: immunofluorescent images of tracked MCs over time representative of three independent experiments. The white outline shows the perimeter of tracked cells using Quimp11b. Far right: perimeter overlay of the same MCs at different time points during live-cell imaging to visualize protrusion dynamics over time. (H) Quantification of total distance traveled and mean speed of co-cultured mTomato^{+} MCs as represented in G. (>600 cells/condition). Data are pooled from independent experiments and are represented as mean ± SD. *n* = 3 biological replicates per group. Distance traveled: *, P = 0.0286. Mean speed: *, P = 0.0286. Mann Whitney *U* test was used. Bars: (A) 20 µm; (B and D) 10 µm; (G) 50 µm. Ctrl, control; rel., relative. See also Videos 1 and 2.

changes upon E-cadherin inactivation were also P-cadherin dependent, as additional shRNA-mediated P-cadherin depletion in *E-cadherin*^{KO} KCs reversed MC dendritic length, MC number, and proliferation to control levels (Fig. 6, C–E). To further ask whether P-cadherin is sufficient or whether MCs require other KC-specific interactions, we used Chinese hamster ovary (CHO) cells stably transfected with P-cadherin. P-cadherin–CHO cells were indeed able to promote expansion of co-cultured MCs, in contrast to wild-type CHO cells, which do not express substantial levels of endogenous P-cadherin (Fig. 6, F and G). In line with this, expression of P-cadherin–GFP in control KCs was sufficient to induce a less dendritic, more flattened MC morphology, mimicking shape changes of MCs contacting *Par3*^{KO} KCs and supporting that P-cadherin mediates heterologous KC–MC interaction (Fig. 6 H). Collectively, these data demonstrate that increased P-cadherin–based adhesion upon loss of Par3 or E-cadherin drives MC dedifferentiation and hyperplasia.

PAR3 and P-cadherin expression and localization in human melanoma

To assess a potential contribution of PAR3 dysfunction and/or P-cadherin overexpression to human disease progression, we studied a panel of skin and melanoma specimens of various tumor grades, including benign nevi, noninvasive melanoma in situ, and early and advanced stages of melanoma. Impor-

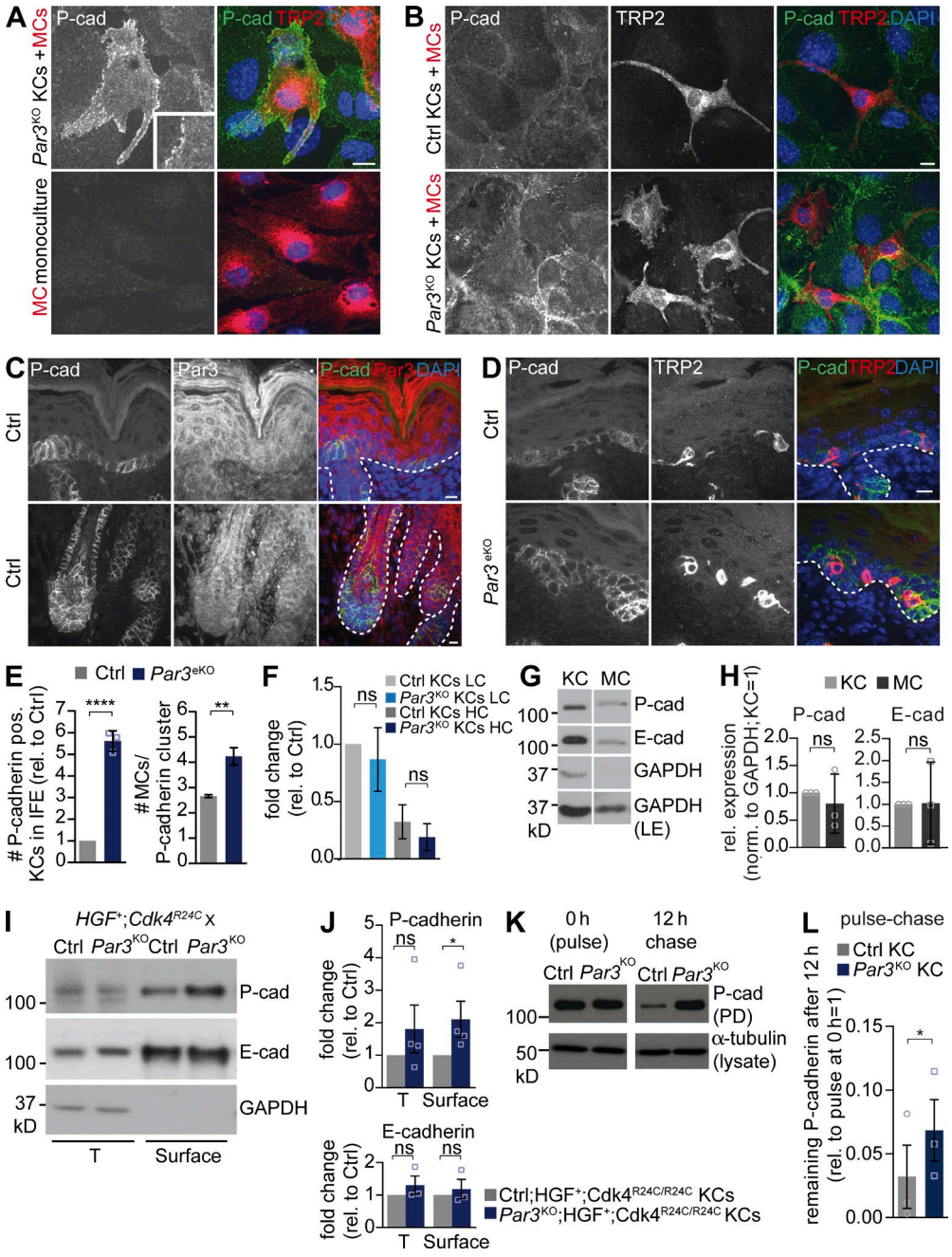

Figure 4. **Par3 loss in KCs increases P-cadherin surface levels and stability and enforces P-cadherin localization to heterologous KC–MC contacts.** (A) P-cadherin immunostaining in *Par3*^{KO} KC–MC co-culture and MC monoculture. Bar, 10 µm. (B) P-cadherin immunostaining in control and *Par3*^{KO} co-cultures. Bar, 10 µm. (C) P-cadherin and Par3 coimmunostainings of neonatal control skin cross sections depicting interfollicular epidermis (top) and hair follicle (bottom) areas. Dashed lines demarcate the MC-containing basal epidermal layer. Bar, 10 µm. (D) P-cadherin and TRP2 immunohistochemistry of neonatal skin cross sections. Dashed lines underline the MC-containing basal epidermal layer. Bar, 10 µm. (A–D) Data are representative of three independent experiments. (E) Quantification of the number of P-cadherin–positive cells in interfollicular epidermis (IFE; data are mean ± SD; $n = 3$ mice per group; ****, $P < 0.0001$; Student's t test) and MC number colocalizing with P-cadherin–positive cell clusters in hair follicles (data are pooled and depicted as mean ± SD; $n = 5$ mice per group; **, $P = 0.0095$; unequal variances Student's t test with Welch's correction). (F) Quantitative RT-PCR for P-cadherin RNA expression in control and *Par3*^{KO} primary KCs cultured at LC or 5 d HC. Data are pooled and represented as mean ± SEM. $n = 5$ biological replicates per group. LC: ns, $P = 0.0940$. HC: ns, $P = 0.941$. One-way ANOVA with Tukey posthoc test was used. (G) Western blot analysis for E- and P-cadherin in total lysates of control MCs and KCs, demonstrating that both cell types express both types of classical cadherins. Data are representative of three independent experiments. (H) Quantification of G. Cadherin levels were first normalized to GAPDH (loading control) before the expression in MCs relative to control KCs was determined. Data are pooled and represented as mean ± SD. $n = 3$ biological replicates per group. Student's t test was used. (I) Biotinylation assay using primary KCs isolated from

tantly, epidermal PAR3 immunoreactivity in areas surrounding invasive primary melanoma was significantly reduced compared with control epidermis (Fig. 7, A and B), in line with our observation that loss of Par3 in KCs drives melanoma. Thus, these results revealed a negative correlation of epidermal PAR3 expression with melanoma progression. Importantly, human P-cadherin robustly localized to heterologous contacts between MCs and surrounding KCs (Fig. 7 C), similar to what we observed in mouse skin (Fig. 4, C and D). Despite sequential dedifferentiation and frequent mislocalization of MCs to suprabasal layers in progressed melanoma, P-cadherin was retained at these KC–MC contacts (Fig. 7, C and D). Quantification of P-cadherin staining intensity revealed significantly increased enrichment of P-cadherin at heterologous contact sites between KCs and MCs, positively correlating with the progression of melanoma (Fig. 7 E). These data suggest that PAR3 dysfunction and enhanced P-cadherin expression at sites of heterologous cross talk correlate with human melanoma progression.

Elevated P-cadherin expression correlates with reduced melanoma patient survival

Interestingly, in line with the data presented in the previous paragraph, in silico analysis of different publicly available datasets from human melanoma confirmed the significant up-regulation of P-cadherin expression in nevi and primary tumors as compared with normal skin (Fig. 8, A and B). The data further revealed reduced P-cadherin expression in distant metastases when compared with primary tumors (Fig. 8, B and C), in agreement with our observation of undetectable P-cadherin levels in mouse melanoma lung metastases (not depicted). Strikingly, however, high P-cadherin expression significantly correlated with reduced melanoma patient survival (Fig. 8 D). Together, these data suggest that P-cadherin is particularly important during initiation, growth, and progression of primary melanoma, whereas melanoma cells may become independent of P-cadherin–mediated effects once the metastatic colonization has occurred.

DISCUSSION

The epidermis constitutes an important niche for other resident skin cells; however, it is largely unknown how the skin epithelium controls the formation and progression of melanoma, a highly lethal nonepithelial malignancy. Here, we identify a non–cell autonomous tumor suppressor role for the polarity protein Par3 through the control of P-cadherin. Our results from genetic mouse models, human melanoma cohorts, and functional co-culture experiments indicate that loss of epidermal Par3 up-regulates cell-surface P-cadherin that serves as a critical determinant to promote not only a pro-proliferative epidermal niche for MCs, but also their gradual transformation, motility, and subsequent dissemination from the primary tumor (Fig. 9). Thus, this study reveals a novel level of complexity in tissue-borne tumor suppression mechanisms, whereby epithelial polarity proteins ensure organismal health through the control of heterologous cell–cell interactions and cytoarchitecture, thus antagonizing the formation and progression of cancers originating from other tissue-resident cell types.

Our findings expose the polarity regulator Par3 as an important rheostat that governs heterologous cell–cell interactions through control of cadherin status. The importance of P-cadherin for human skin biology is highlighted by two genodermatoses that are associated with congenital alopecia and linked to *CDH3* loss-of-function mutations or deletions interfering with P-cadherin–mediated adhesion (Souied et al., 1995; Sprecher et al., 2001; Indelman et al., 2002; Kjaer et al., 2005). Consistent with this, P-cadherin down-regulation in cultured human skin resulted in altered hair growth and, interestingly, a reduction of hair follicle cells positive for MC markers (Samuelov et al., 2012, 2013). *P-cadherin* deletion in mice results in premature differentiation of mammary glands (Radice et al., 1997), but no overt skin phenotype was reported, perhaps because of the functional compensation by E-cadherin (Tinkle et al., 2008; Michels et al., 2009). Whether and how aberrant P-cadherin affects MC shape, transformation, and melanoma progression has not been demonstrated. Our results now identify a novel protumorigenic function of P-cadherin in melanoma and highlight that this classical cadherin is a key mediator of interactions between epithelial KCs and neural crest–derived cells important in the context of skin cancer formation and progression.

The Par3-dependent control of surface P-cadherin appears to involve a direct regulation of P-cadherin protein function. Though induction of P-cadherin mRNA downstream of p63 (Osada et al., 2005; Shimomura et al., 2008) or as consequence of E-cadherin deletion (Chen et al., 2014) has been reported, loss of Par3 in KCs did not result in elevated P-cadherin mRNA expression. Instead, our surface labeling and pulse-chase experiments strongly suggest that Par3 counteracts the stability of surface-localized P-cadherin. Though ectodomain cleavage is a common mechanism for cadherin

ctrl;HGF^{+};$Cdk4^{R24C/R24C}$ and $Par3^{eKO}$;HGF^{+};$Cdk4^{R24C/R24C}$ mice, 3 d after calcium switch, demonstrating elevated P-cadherin surface levels in Par3-deficient KCs. (J) Quantification of I. P-cadherin levels were normalized to GAPDH (loading control) before fold-changes relative to control cells were determined. Data are pooled and depicted as mean ± SEM. P- cadherin: $n = 4$ biological replicates per group; *, P = 0,0286; Mann Whitney *U* test. E- cadherin: $n = 3$ biological replicates per group. T: ns, P = 0.335; Surface: ns, P = 0.567; Student's *t* test. (K) Immunoblot analysis of surface biotin-labeled P-cadherin stability in control and $Par3^{KO}$ KCs cultured at 2 d HC. (L) Quantification of K. P-cadherin levels at 12-h chase period (after biotinylation) were normalized to total P-cadherin expression per genotype at 0 h (= pulse). Data are pooled and represented as mean ± SEM. $n = 3$ biological replicates per group. *, P = 0.0327; Student's *t* test. Cad, cadherin; Ctrl, control; LE, long exposure; norm., normalized; PD, pull-down; pos., positive; rel., relative; T, total protein.

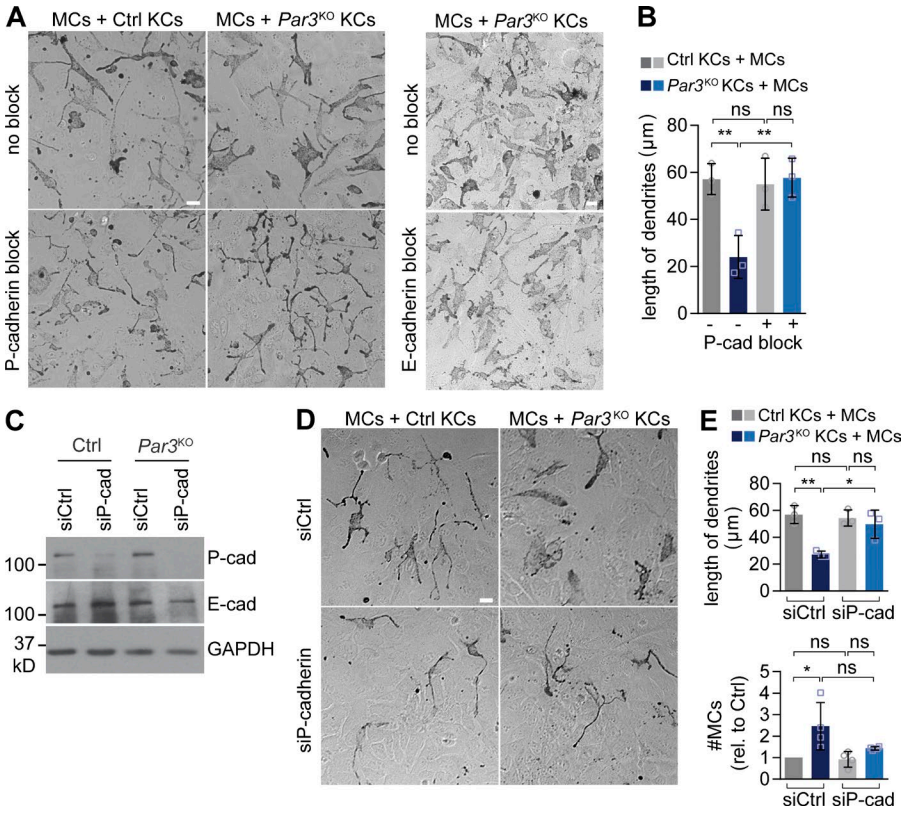

Figure 5. **P-cadherin is required for MC dedifferentiation and hyperplasia upon loss of epidermal Par3.** (A) Antibody-mediated P-cadherin block (left) but not E-cadherin block (right) in direct co-culture restores MC dendricity in MCs co-cultured with *Par3*^{KO} KCs. Bars, 20 µm. Data are representative of three independent experiments. (B) Quantification of A (>10 images per condition). Data are pooled and represented as mean ± SD. $n = 3$ biological replicates per group. **, P = 0.0079 and 0.0071; ns, P = 0.9691 and 0.8514; one-way ANOVA with Tukey posthoc test. (C) Western blot analysis for P- and E-cadherin expression in control and *Par3*^{KO} KCs after siRNA transfection, confirming efficient P-cadherin knockdown. Data are representative of three independent experiments. (D) siRNA-based P-cadherin knockdown (bottom) restores shape and dendritic length of MCs in direct co-culture with *Par3*^{KO} KCs. Bar, 20 µm. Data are representative of four independent experiments. (E) Quantification of D (>15 images per condition). Data are pooled and represented as mean ± SD. Dendritic length: $n = 3$ biological replicates per group; *, P = 0.0184; **, P = 0.0038; one-way ANOVA with Tukey posthoc test. MC number: $n = 4$ biological replicates per group; *, P = 0.0179; ns, P = 0.617; one-way ANOVA with Tukey posthoc test. cad, cadherin; Ctrl, control; rel., relative.

regulation (Cavallaro and Dejana, 2011), by different biochemical assays including concanavalin A or TCA-mediated precipitation of proteins in culture supernatants, we did not obtain evidence for significant P-cadherin shedding in KCs of either genotype (not depicted). Therefore, we conclude that Par3 controls P-cadherin surface levels by alternative mechanisms that may include promoting P-cadherin internalization or restricting the incorporation of P-cadherin into cell–cell contacts. An essential cadherin surface retention factor is the armadillo protein p120catenin (p120ctn; Ireton et al., 2002; Davis et al., 2003; Xiao et al., 2003). Binding of p120ctn to the juxtamembrane domain of classical cadherins can prevent cadherin endocytosis, thereby increasing cadherin surface levels, clustering, and adhesive strength (Yap et al., 1998). These data provide a foundation for future work to investigate the largely unknown regulatory mechanisms that coordinate heterologous cell–cell interactions in tissue homeostasis and malignant transformation.

Intriguingly, we found that, in the skin epidermis, Par3 selectively controls P-cadherin but not E-cadherin expression, the more abundant classical cadherin expressed in this tissue. In agreement, and in contrast to P-cadherin, blocking E-cadherin–mediated adhesion was indeed not able to reverse the abnormal morphology of MCs co-cultured with Par3-deficient KCs. Instead, *E-cadherin*^{KO} KCs mimicked *Par3*^{KO} KCs with respect to their effect on MC shape and proliferation, which we show could be attributed to elevated P-cadherin. Interestingly, previous studies reported impaired E-cadherin–based cell–cell cohesion in Par3-depleted breast tumor cells (Xue et al., 2013) and Par3/Bazooka-dependent roles of E-cadherin in *Drosophila* adherens junction formation and collective migration (Campbell and Casanova, 2015). Thus, this suggests that Par3-mediated control of distinct classical cadherins might be context specific. Whereas earlier studies indicated a role for E-cadherin in mediating KC–MC adhesion under homeostatic conditions (Tang et al., 1994; Kuphal et al., 2004; Wagner et al., 2015), our work suggests a functional cadherin switch whereby MC hyperplasia and transformation upon loss of Par3 is predominantly driven by P-cadherin and not E-cadherin.

Par3 loss-dependent up-regulation and stabilization of P-cadherin in the epidermal environment stimulates MC proliferation and impairs the formation of dendrites, a hallmark of differentiated MCs. This is accompanied by an increase in MC protrusive activity, migration, and metastatic spread to the lungs, suggesting that elevated P-cadherin function unleashes a permissive niche for MC transformation, invasion, and metastasis. Notably, our findings are supported by physiological events in mammalian development: P-cadherin is abundantly expressed in cell types that intimately commu-

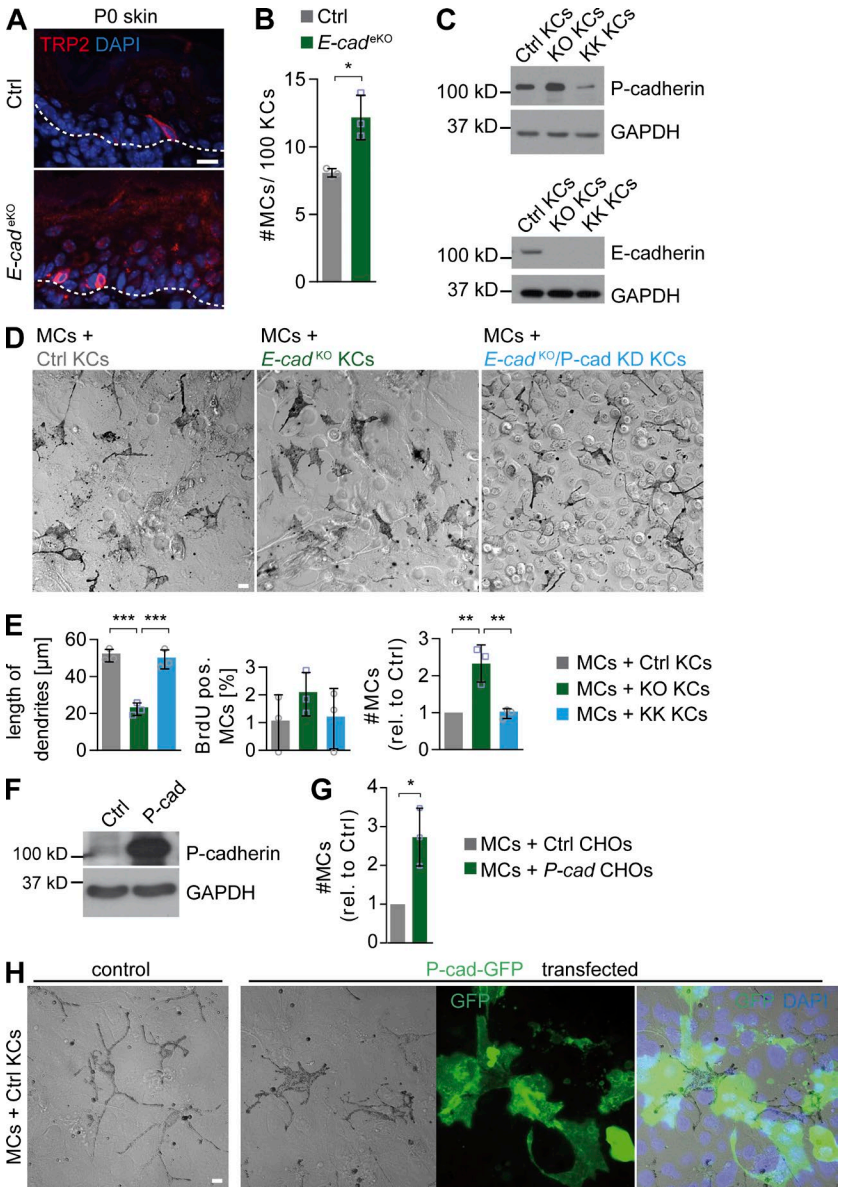

Figure 6. **P-cadherin expression is sufficient to induce MC dedifferentiation and hyperproliferation.** (A) TRP2 immunostaining of back skin cross sections of P0 control and *E-cad*^{eKO} mice. Data are representative of three independent experiments. (B) Quantification of MC number in interfollicular epidermis of control and *E-cad*^{eKO} P0 back skin. Data are pooled and represented as mean ± SD. $n = 3$ mice per group. *, P = 0.0133; Student's *t* test. (C) Western blot analysis for P- and E-cadherin expression in control, *E-cad*^{KO} (KO), and *E-cad*^{KO}/P-cad^{KD} (KK) KCs. Data are representative of three independent experiments. (D) Phase-contrast micrographs of MCs co-cultured with control (left), *E-cad*^{KO} (middle), or *E-cad*^{KO}/*P-cad*^{KD} (right) KCs for 3 d at HC. Data are representative of three independent experiments. (E) Quantification of D (eight images per condition). Data are pooled and represented as mean ± SD. Dendritic length: $n = 3$ biological replicates per group; Ctrl versus KO: ***, P = 0.0003; KO versus KK: ***, P = 0.0005; one-way ANOVA with Tukey posthoc test. MC numbers: $n = 3$ biological replicates per group; Ctrl versus KO: **, P = 0.0038; KO versus KK: **, P = 0.0042; one-way ANOVA with Tukey posthoc test. (F) Western blot analysis for P-cadherin in control- and P-cadherin–expressing CHOs. Data are representative of two independent experiments. (G) Quantification of MC number co-cultured with control or P-cadherin overexpressing CHO cells for 4 d at HC (20 images per condition). Data are pooled and represented as mean ± SD. $n = 3$ biological replicates per group. *, P = 0.0159; Student's *t* test. (H) Co-culture of MCs with control- or P-cadherin–GFP–transfected control KCs. Data are representative of two independent experiments. Bars: (A) 10 µm; (D and H) 20 µm. cad, cadherin; Ctrl, control; pos., positive; rel., relative.

nicate with adjacent tissues and possess a high migratory potential, such as in the apical ectodermal ridge and the hair follicle placode important for down-growth of the follicle epithelium (Shimomura et al., 2008). In the tumor context, although both pro- and antitumorigenic roles for intrinsic P-cadherin have been proposed (van Roy, 2014; Ribeiro and Paredes, 2015), the invasion of various cancer cell lines is promoted by P-cadherin expression (Paredes et al., 2004; Taniuchi et al., 2005; Mandeville et al., 2008; Cheung et al., 2010; Kümper and Ridley, 2010). This suggests that P-cadherin can mediate proinvasive behavior both during development and in malignant disease.

We show that in human melanoma, P-cadherin up-regulation at heterologous junctions between KCs and intraepidermal melanoma cells is already detectable in smaller premalignant lesions. This suggests that aberrant P-cadherin–mediated interaction of MCs with the surrounding epithelium is an early event in melanomagenesis. This view is supported by the P-cadherin expression profiles obtained from several large human melanoma databases that revealed an initial increase of P-cadherin expression in nevi and primary melanoma, whereas P-cadherin expression appears to decline once a metastasis has colonized. Strikingly, high P-cadherin expression in melanoma was associated with decreased melanoma patient survival, underpinning the potential of P-cadherin as a prognostic marker in melanoma. Collectively, we assume an early requirement for P-cadherin in melanoma formation and invasion: combining our results obtained from in vivo and in vitro analyses of mouse and human melanoma, we postulate that high levels of

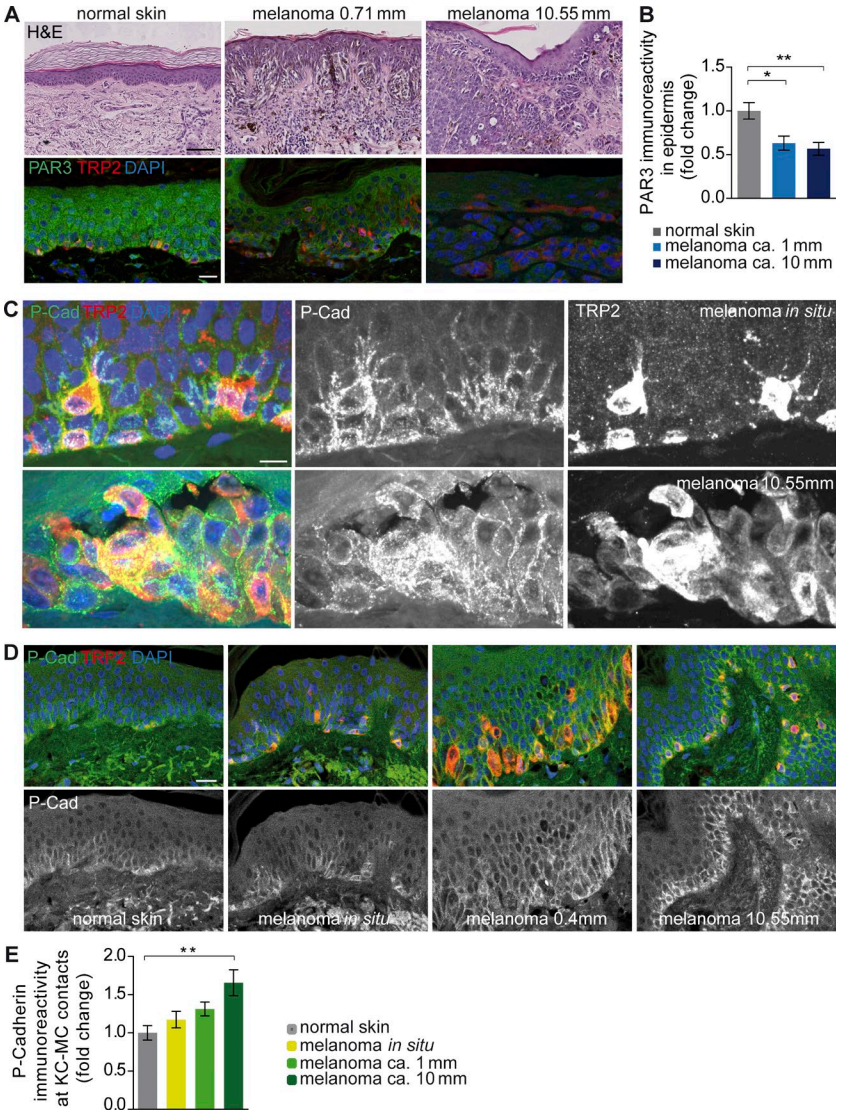

Figure 7. **Reduced epidermal PAR3 and increased P-cadherin levels at heterologous contacts correlate with progression of human melanoma.** (A) H&E staining (top) and PAR3 and TRP2 immunostainings (bottom) of human normal skin and melanoma tissue. Bars: (top) 100 µm; (bottom) 20 µm. Data are representative of at least three independent experiments. (B) Quantification of epidermal anti-PAR3 immunoreactivity in normal skin epidermis (n = 10 tissues from different donors), melanoma with tumor depth ∼1 mm (n = 9 tumors from different patients), and melanoma with tumor depth ∼10 mm (n = 8 tumors from different patients). Data are mean + SEM. *, P = 0.0113; **, P = 0.0040; one-way ANOVA with Tukey posthoc test. (C) P-cadherin and TRP2 costaining in melanoma in situ and melanoma with ∼10 mm depth revealing high levels of P-cadherin at sites of KC–MC contacts. Bar, 10 µm. Data are representative of at least three independent experiments. (D) P-cadherin immunostainings of human normal skin and melanoma tissue. Bar, 20 µm. Data are representative of at least three independent experiments. (E) Quantification of anti–P-cadherin immunoreactivity in melanoma patients in KC–MC contacts of normal skin epidermis (n = 9 tissues from different donors), melanoma in situ (n = 9 tissues from different patients), melanoma with tumor depth ∼1 mm (n = 8 tumors from different patients), and ∼10-mm melanoma (n = 4 tumors from different patients). Data are pooled and depicted as mean + SEM. **, P = 0.0054; one-way ANOVA with Tukey posthoc test. cad, cadherin.

P-cadherin mediate heterologous KC–MC interactions as long as melanoma cells are in direct contact with the (Par3 deficient) skin epithelium but that tumor cells become independent of P-cadherin once they have left the epidermal niche and colonize at distant sites, potentially switching to other types of adhesive interactions. Such niche-dependent P-cadherin function in melanoma would be in agreement with a transient up-regulation of P-cadherin during breast cancer formation that has recently been associated with an intermediate, metastable cancer cell population prone to tumor progression, and P-cadherin levels are also reduced in breast cancer metastases (Ribeiro and Paredes, 2015). P-cadherin is up-regulated in ∼30% of human invasive carcinoma and associated with low differentiation (Imai et al., 2008; Ribeiro and Paredes, 2015). In breast cancer, P-cadherin serves as an important clinical prognostic factor, with ∼25% of these tumors harboring *CDH3* gene amplifications (cBioPortal; Eirew et al., 2015), and there is a strong correlation of P-cadherin expression with poor patient survival, invasion, and distant metastasis (Peralta Soler et al., 1999; Gamallo et al., 2001; Paredes et al., 2005; Liu et al., 2012). Thus, our results agree with an emerging proinvasive function of P-cadherin and expand this concept by identifying P-cadherin as a crucial mediator of tumor–microenvironmental cross talk.

Next to diagnostic perspectives, the reduction of epidermal Par3 levels and the up-regulation of P-cadherin with melanoma progression have several additional clinical implications. Because of its surface expression, targeting P-cadherin to disrupt aberrant cell–cell adhesion in tumorigenesis seems promising. For example, after sunburn, blocking P-cadherin could potentially reduce the risk of MC transformation and instead allow the clearance of cells that acquired mutations. Interestingly, short P-cadherin extracellular fragments have been reported to promote both breast cancer and melanoma cell migration (Bauer and Bosserhoff, 2006; Ribeiro et al., 2010), further substantiating that P-cadherin

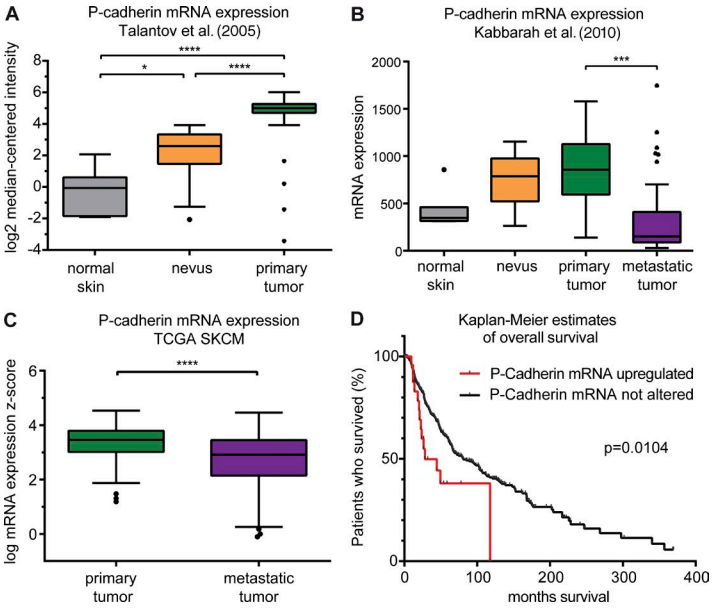

Figure 8. **Human P-cadherin expression is associated with melanoma formation, progression, and reduced patient survival.** (A) RNA expression profiling by microarray of human normal skin (n = 7 tissues from different donors), nevi (n = 18 tissues from different donors), and primary melanoma (n = 45 tumors from different patients) reveals increasing P-cadherin mRNA expression with tumor progression. Error bars: 95% confidence interval (Tukey's posthoc test). *, P = 0.0152; ****, P < 0.0001; one-way ANOVA with Tukey's posthoc test. The dataset is published by Talantov et al. (2005) under GEO accession no. GSE3819. (B) Profiling of mRNA expression (no. VALUE = MAS5 — calculated signal intensity after global scaling the mean intensity to 600) by microarray of normal skin (n = 7 tissues from different donors), nevi (n = 9 tissues from different donors), primary melanoma (n = 31 tumors from different patients), and metastatic melanoma (n = 73 tumors from different patients) reveals a trend of increasing P-cadherin mRNA expression with tumor progression, whereas P-cadherin mRNA levels are significantly reduced in metastatic samples compared with primary melanoma samples (95% confidence interval; Tukey's posthoc test). ***, P = 0.001; one-way ANOVA with Tukey's posthoc test. The dataset is published by Kabbarah et al. (2010) under GEO accession no. GSE46517. (C) P-cadherin mRNA expression is significantly increased in primary melanoma (n = 103 tumors) compared with metastatic melanoma (n = 368 tumors). 95% confidence interval (Tukey's posthoc test). ****, P < 0.0001; Student's t test. The Cancer Genome Atlas (TCGA) skin cutaneous melanoma (SKCM) dataset was used. (D) Patients with P-cadherin mRNA up-regulation (total n = 25 patients; number of cases deceased = 14) have worse overall survival compared with patients without alterations in P-cadherin expression (total n = 434 patients; number of cases deceased = 205). Median months survival: cases with P-cadherin alteration, 28.15 mo; cases without alteration, 81.14 mo. Up-ticks represent censored cases. P = 0.0104; log-rank (Mantel-Cox) test. TCGA SKCM dataset was used.

inhibition may be a viable strategy for anticancer therapy. In fact, antitumor and antimetastatic properties of an anti–P-cadherin antibody, PF-03732010 (Pfizer), have been demonstrated in several carcinoma mouse models (Zhang et al., 2010; Park et al., 2012), and a recent clinical trial (ClinicalTrials.gov accession no. NCT00557505) revealed that this antibody is well tolerated in humans, although the efficacy in human cancer still requires further investigation. Intriguingly, our analyses also revealed significantly increased ERK and Akt activation accompanied by increased tumor cell proliferation in melanomas of *Par3*^{eKO}*;HGF;Cdk4*^{R24C} mice. This indicates that Par3 loss non–cell autonomously promotes growth and survival signaling in MCs through regulation of these pathways. Although the exact upstream signaling events remain to be investigated in future work, these data open the possibility that inhibition of ERK (e.g., by MEK inhibitors already approved for clinical use) and Akt signaling might represent another viable strategy for treatment of Par3- or P-cadherin–dysregulated melanoma, next to P-cadherin–tailored approaches.

Collectively, we show a novel mechanism of heterologous communication between key skin-resident cell populations that depends on a subset of classical cadherins and is controlled by the conserved polarity protein Par3. The hitherto unknown role of epidermal Par3 to counteract the function of P-cadherin and to dictate the cytoarchitecture of neighboring MCs in their epidermal niche highlights that molecular control of cyto- and tissue architecture is not only important for intrinsic cell polarity, but also crucial to suppress malignant disease stemming from neighboring tissue-resident cell types.

MATERIALS AND METHODS

Human subjects

The use of human specimen involved in this study was approved by the institutional review board at the Medical Faculty of the University of Cologne (file reference 12–163). All samples were collected with informed consent of the donors, and studies were conducted in accordance with the principles of the Declaration of Helsinki and with institutional review board policies and procedures for research dealing with tumor specimen.

Animals

Mice with epidermal *Par3* deletion have been described previously (*K14Creneo*KI$^{+/wt}$;*Par3*$^{fl/fl}$; Iden et al., 2012). These were crossed to *HGF/SFxCdk4*$^{R24C/R24C}$ mice (Tormo et al., 2006), *H2B–enhanced GFP* (*EGFP*) mice (Hadjantonakis and Papaioannou, 2004), and double-fluorescent *mT/mG* reporter mice (Muzumdar et al., 2007). All animals were on C57BL/6J background. Mice were housed and fed according to federal guidelines. Genetically modified mice were provided by W. Birchmeier (Max-Delbrück Center for Molecular Medicine, Berlin, Germany), S. Ohno (Yokohama City University, Yokohama, Japan), G. Merlino (National Cancer Institute, Bethesda, MD), and M. Barbacid (Spanish National Cancer Research Center, Madrid, Spain). All animal experi-

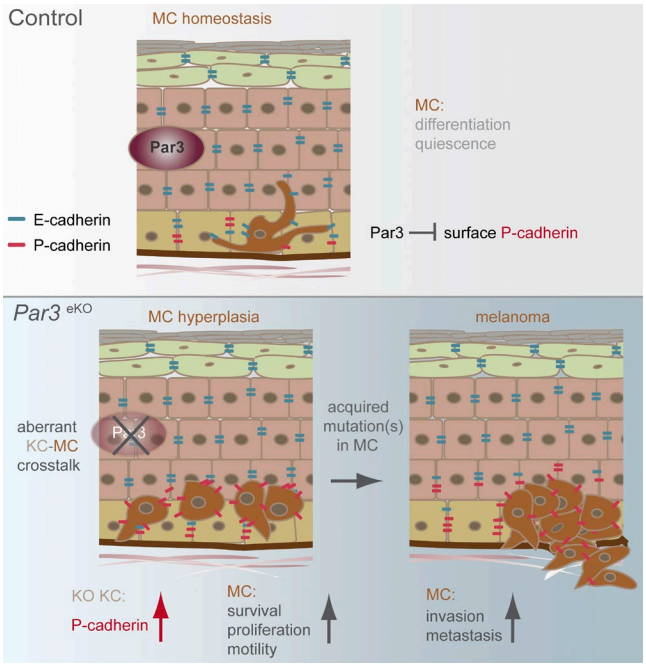

Figure 9. **Hypothetical model.** The epidermal polarity protein Par3 is an important non-cell autonomous suppressor of melanoma. (Top) Epidermal Par3 controls MC homeostasis by restricting P-cadherin–mediated KC–MC communication and thus promoting differentiated MC cytoarchitecture. (Bottom) Loss of KC Par3 leads to reduced dendritic length and increased motility, proliferation, and survival of MCs, phenotypes mediated by increased stability, and surface localization of P-cadherin in KCs. Thus, through direct KC–MC interaction, augmented P-cadherin establishes a permissive niche for MC dedifferentiation, transformation, and invasion when polarity protein function in the epidermal microenvironment is impaired (bottom, right).

ments were performed according to institutional guidelines and local governmental authorities of the State Office North Rhine-Westphalia, Germany (Landesamt für Natur, Umwelt und Verbraucherschutz Nordrhein-Westfalen).

Antibodies

The following antibodies were used in this study: rabbit antibodies directed against Par3 (no. 07-330; EMD Millipore), cleaved caspase3 (no. 9661; Cell Signaling Technology), phospho-Akt (Ser 473; 4060; Cell Signaling Technology), phospho-p44/42 MAPK (Erk1/2; Thr202/Tyr204; no. 4370; Cell Signaling Technology), rat anti–P-cadherin (PCD-1; no. 13-2000Z; hybridoma supernatant; Invitrogen; Nose and Takeichi, 1986), E-cadherin/DECMA-1 (no. 147302; BioLegend; Vestweber and Kemler, 1985), mouse anti–P-cadherin (no. 610228; BD), GAPDH (no. MAB374; EMD Millipore), α-tubulin (no. T-5168; clone B-5-1-2; Sigma-Aldrich), BrdU (no. MO744; Dako), E-cadherin (no. 610181; BD), β-catenin (no. 610154; BD), PCNA (no. NA03; clone PC10; EMD Millipore), and goat anti-TRP2 (no. sc-10451; Santa Cruz Biotechnology, Inc.). For secondary detection, Alexa Fluor 488 and 568 (Molecular Probes) or horse radish peroxidase (GE Healthcare) conjugates were used.

Skin tumorigenesis experiments

Biometric planning with consideration of effect size, variation, and type 1 and type 2 errors was performed to determine the required group sizes in animal experiments ensuring adequate power. Only initially healthy and normally weighed mice were used for experiments. Both male and female mice were included, whereby the male/female ratio was comparable in control and test groups, and for randomization, mice of different genotypes were cohoused. Melanoma experiments were performed with 8-wk-old *K14Creneo*KI$^{wt/wt}$;*Par3*$^{fl/fl}$;*HGF*$^{+}$;*Cdk4*$^{R24C/R24C}$ (Ctrl;*HGF*$^{+}$;*Cdk4*$^{R24C/R24C}$) and *K14Creneo*KI$^{+/wt}$;*Par3*$^{fl/fl}$;*HGF*$^{+}$;*Cdk4*$^{R24C/R24C}$(*Par3*^{eKO};*HGF*$^{+}$;*Cdk4*$^{R24C/R24C}$). Mice were dorsally shaved and treated the next day with a single dose of 25 µg DMBA in 200 µl acetone. Melanoma numbers and sizes were documented weekly in blinded fashion. When melanomas exceeded sizes of 15 mm or when signs of illness were observed, mice were sacrificed and examined. Skin melanomas were excised, and internal organs (including lymph nodes, liver, spleen, brain, and kidney) were snap frozen or paraformaldehyde (PFA) fixed for further analyses. Lungs were PFA perfused, and macroscopically visible metastases were counted. Two-stage DMBA/TPA treatment was performed as previously described (Iden et al., 2012).

Isolation and immunohistochemistry of tail epidermis whole mounts

Whole mounts were prepared according to Braun et al. (2003). In brief, tail epidermis was separated from dermis by 4-h incubation in 5 mM EDTA/PBS at 37°C and fixed in 4% PFA/PBS for 1 h at room temperature. Tissue was blocked for 1 h in PB buffer (0.9% NaCl and 20 mM Hepes, pH 7.2, plus 0.5% skim milk powder, 0.25% fish skin gelatin [Sigma-Aldrich], and 0.5% Triton X-100), primary antibody incubation was performed in PB buffer at room temperature overnight, and after 5× washing in 0.2% Tween/PBS for 1 h, whole mounts were stained with secondary antibodies at room temperature overnight. After washing, whole mounts were mounted in Mowiol.

Tissue processing, histology, and immunohistochemistry

Hematoxylin and eosin (H&E) staining and immunohistochemistry of normal skin and skin tumors were performed on PFA-fixed 7-µm paraffin sections. H&E stainings were mounted in Entellan medium (Merck). For immunofluorescence staining of tissues, paraffin sections were deparaffinized. Heavily pigmented melanomas were bleached by incubation in 30% H_2O_2 and 0.5% KOH at 37°C for 20 min followed by 1% acetic acid (20 sec) and 1 M Tris HCl, pH7.5, for 5 min at room temperature. Antigens were retrieved by boiling in pH 6 buffer (1.8 mM citric acid and 8.2 mM sodium citrate) for 20 min. After washing and 2-h blocking (10% normal donkey

serum/PBS) at room temperature, primary antibodies were applied overnight at 4°C in a humidified chamber. Alexa Fluor–conjugated secondary antibodies and DAPI (Invitrogen) were incubated for 1 h at room temperature in antibody buffer before washing and mounting in Mowiol.

Isolation of primary mouse MCs and KCs

Primary mouse MCs were isolated from epidermis of newborn control mice and maintained up to passage 3. To separate epidermis from dermis, whole skins of P0-P3 mice were incubated in 5 mg/ml Dispase II (Sigma-Aldrich) diluted in RPMI640 medium (Gibco) plus 10% FCS-Gold (Biochrom), 100 IU/ml penicillin/streptomycin, 100 nM sodium pyruvate, and 10 mM nonessential amino acids (all Gibco) at 4°C overnight (RPMI medium hereafter). After 20-min incubation of the epidermis in TrypLE (Gibco) at room temperature, dissociated cells were collected and cultured in RPMI medium containing 200 nM TPA and 200 pM cholera toxin (both Sigma-Aldrich). Passage 0 cultures contained nonpigmented melanoblasts, MCs, and KCs, and after 1 wk, small colonies of dendritic MCs appeared. Because of terminal differentiation, KCs were absent after first passage, resulting in MC monocultures. Primary mouse KCs were isolated from the epidermis of newborn Ctrl;HGF^{+};$Cdk4^{R24C/R24C}$ and $Par3^{eKO}$;HGF^{+};$Cdk4^{R24C/R24C}$ mice as described for primary MC cultures. Mixed litters were used to isolate control and KO cells. KCs were plated on collagen I–coated dishes and cultured in minimal Ca^{2+} medium (50 µM Ca^{2+}; custom made DMEM/Ham's F12; Biochrom; FAD medium).

Direct and indirect KC–MC co-cultures

For direct co-cultures, control and $Par3^{KO}$ KCs and MCs were either seeded directly in the ratio 5:1 in KC FAD growth medium to be 100% confluent the next day and ready for Ca^{2+} switch (1.8 mM; HC). Alternatively, KCs were seeded in KC FAD growth medium, and MCs were added later. Co-cultures were performed for up to 10 d. For indirect co-cultures, MCs were seeded at subconfluency on collagen I–coated TransWell permeable filter supports (TransWell Clear; 0.4 µm pore size; 6.5 mm diameter; Corning) and incubated in 24-well plates harboring control or $Par3^{KO}$ KCs. Indirect co-cultures were grown for up to 9 d in FAD (LC) or RPMI (HC) medium, which was refreshed twice per week. MC numbers were determined by TRP2 immunostaining of PFA-fixed cells.

Quantification of PAR3 and P-cadherin expression in human tissue sections

Human tissue sections of different melanoma stages were processed for immunostaining as described in the Tissue processing, histology, and immunohistochemistry section. Micrographs of PAR3 and P-cadherin immunostainings were captured using the gSTED Super-resolution and confocal microscope (Leica Biosystems) at nonsaturated detection levels and identical imaging conditions among healthy epidermal and melanoma areas. PAR3 or P-cadherin immunoreactivity was quantified using Application Suite X software (Leica Biosystems; three different regions of interest per tissue section; minimum of three sections per specimen).

Live-cell imaging of co-cultures and antibody-blocking studies

For live-cell imaging, co-cultures were seeded on microscopy chambers (µ-Slide 8-well ibiTreat; Ibidi) to be confluent and Ca^{2+} switched the next day. After 48-h calcium switch, blocking antibodies were applied (PCD-1 hybridoma supernatant or anti–E-cadherin DECMA-1; 50 µg/ml), and cells were imaged every 7 min for up to 7 h at 37°C and 5% CO_2 using a microscope (Meta Confocal 510; ZEISS) and analyzed using ImageJ (National Institutes of Health).

Live-cell imaging of co-cultures for membrane tracing and analysis of MC motility

For membrane tracing and analysis of MC motility, MCs expressing fluorescent membrane-targeted Tomato were co-cultured with subconfluent primary or spontaneously immortalized KCs on µ-Slides (Ibidi) and Ca^{2+} switched the next day. After 3–4 d in HC, slides were imaged every 15 min for 12 h using an epifluorescence microscope (DM6000B; Leica Biosystems; 20× air objective) at 28 positions each (MCs + control or $Par3^{KO}$ KCs; 37°C and 5% CO_2). Image sequences were background subtracted and despeckled, a gaussian filter ($\sigma = 1$) was applied in ImageJ, and the sequences were subsequently analyzed with the Quimp11b plug-in for membrance tracing and tracking of individual MCs in co-cultures (>600 cells/condition). Output results from the Quimp11b analysis were consolidated using an R script.

Cells

The following cells were used in this study: primary KCs isolated from *K14-Cre*$^{+/wt}$;*Par3*$^{flox/flox}$;*HGF;Cdk4*^{R24C} mice, primary MCs isolated from *H2B-GFP* or *mT/mG* mice, primary control, *K14Cre*$^{+/wt}$;*Ecadherin*$^{fl/fl}$ (*E-cad*^{KO}; Tunggal et al., 2005), *E-cadherin*^{KO}/shP-cadherin KCs (*E-cad*^{KO}/P-cad^{KD}; Michels et al., 2009), spontaneously immortalized control and $Par3^{KO}$ KCs, and control or mouse P-cadherin overexpressing CHO cells. All cell isolations and lines used in this study were validated by immunoblotting for loss of function or gain of function of genes of interest as well as for expression of KC- or MC-specific markers and, in case of knockout cells, additionally by PCR genotyping from genomic DNA. Litters were derived from multiple parental breedings. Cultured cells were regularly monitored for mycoplasma contamination and discarded in case of positive results.

Plasmids and transfections

The P-cadherin expression construct with C-terminal fusion of *EGFP* was generated by amplification of mouse *P-cadherin* from cDNA with primers introducing restriction sites for HindIII (5′-ACGTAAGCTTATGGAGCTTCTTAGTGG GCC-3′) and BamHI (5′-ATATGGATCCGTCATCCT

CACCGCCACCAT-3′) via PCR (high fidelity polymerase; Roche). The HindIII- and BamHI-digested PCR product and pEGFP-N3 were ligated using T4 DNA ligase (NEB). For ectopic P-cadherin–EGFP expression, 90% confluent KC monolayers or co-cultures were transfected using Viromer RED (lipocalyx) according to the manufacturer's protocol.

Proliferation and survival analyses of co-cultured MCs

Co-cultures were incubated with 160 µg/ml BrdU (Roche) and PFA fixed 3 h later. For permeabilization, fixed cells were incubated with 0.5% Triton X/2N HCl. Immunofluorescence staining with anti-BrdU and anti–cleaved caspase3 antibodies was followed by quantification of proliferating and apoptotic MCs in co-cultures from a minimum of 20 random phase-contrast microscopy micrographs (ImageJ).

Immunofluorescence analysis of cells

Mono- or co-cultures were seeded on collagen I–coated 8-well or 16-well LabTek Chamber slides (Thermo Fisher Scientific), grown until confluency, and Ca^{2+} switched to HC (1.8 mM). Immunofluorescence stainings were performed as described previously (Iden et al., 2012).

Image acquisition and analysis

H&E-stained tissue sections were scanned using an automated slide scanner (Leica Biosystems; 40× air objective) and analyzed using corresponding viewer software (SlidePath Digital Image Hub; Leica Biosystems). For details on live-cell imaging, see the separate Materials and methods sections. Micrographs of immunofluorescent samples were captured using a spinning disk confocal microscope (PerkinElmer; 20× air objective; 63× objective with oil immersion), a confocal microscope (TCS SP8 gSTED; Leica Biosystems; 20× air objective; 63× objective with oil immersion), or an epifluorescence microscope (DM6000B; Leica Biosystems; 20× air objective; 63× objective with glycerol immersion), and analysis was performed using ImageJ, Volocity (PerkinElmer), Illustrator (Adobe), CellProfiler (Broad Institute), and the Quimp11b plug-in (Tyson et al., 2014; Bretschneider laboratory) for ImageJ and Rstudio. Experimental mice and whole dissected organs were documented using a digital single-lens reflex camera (D5100; Nikon) equipped with an AF-S 18-55 mm objective (Nikon) or AF90 mm objective (Tamron) for macromode.

Quantification of MC number and morphology in co-cultures

The cell counter plugin and freehand line tool of ImageJ were used for quantification of MC number and dendritic length in co-cultures. MC size and morphology micrographs were quantified using CellProfiler software (Carpenter et al., 2006): threshold for nuclei segmentation was manually determined in test mode and the following steps were performed automatically without user intervention on all images: (a) the intensity of the images was rescaled by each image's maximum, (b) the green channel was extracted from each color image, (c) an illumination function was calculated and applied to correct uneven illumination for each image, (d) cell nuclei were segmented from the background using a global threshold strategy and identified as primary objects, (e) identified nuclei were used as seed regions to identify the rest of the cell, and (f) the size and morphological features of identified cells were measured.

Quantitative RT-PCR

For quantitative RT-PCRs, RNA was isolated from tumor tissue, normal skin, or cells using TRIzol reagent according to the manufacturer's protocol (Invitrogen). RNA was reversely transcribed using a QuantiTect Reverse Transcription kit (QIAGEN) and amplified with TaqMan Universal PCR Master Mix. Probes for target genes were ordered from TaqMan Assay-on-Demand kits (*Rn18s* Mm03928990_g1 and *Cdh3* Mm01249209; Applied Biosystems).

SiRNA-mediated P-cadherin down-regulation

Subconfluent KCs were transfected with 100 nM ON-TAR GETplus SmartPool against P-cadherin and the nontargeting control pool (mouse Cdh3 no. L-063520-01 and no. D-001810-10-05; Thermo Fisher Scientific) using X-tremeGENE siRNA Transfection reagent (Roche) according to the manufacturer's protocol. P-cadherin down-regulation was validated by Western blot analysis and was most efficient between 24 and 72 h after transfection.

Preparation of cell extracts, SDS-PAGE, and immunoblotting

Total cell lysates were prepared in hot SDS buffer (1% SDS and 10 mM EDTA). After determination of protein concentrations via bicinchoninic acid assay (Thermo Fisher Scientific), lysates were boiled in SDS sample buffer for 5 min. Separation by SDS-PAGE (NuPAGE; Invitrogen or 10% self-made) and immunoblotting were performed according to standard procedures.

Preparation of melanoma extracts for immunoblot analysis

For protein biochemical analysis, snap-frozen tissue of individual melanoma was minced and transferred to ice-cold lysis buffer (150 mM NaCl, 50 mM Tris/HCl, pH7.4, 1 mM EDTA, and 0.5% (vol/vol) Triton X-100, supplemented with 2 mM NaF, 25 mM β-glycerophosphate, 0.1% SDS, 1 mM dithiothreitol, and protease inhibitor cocktail [no. P8340; 1:1,000; Sigma-Aldrich]). The tissue was dissociated for 3 min at 30 Hz using a tissue homogenizer (mixer mill 300; QIAGEN), incubated for 10 min on ice, and then cleared by centrifugation for 10 min at 4°C and 13,000 rpm. Further processing was performed as described for extracts of cultured cells.

Proliferative index of mouse melanoma cells in vivo

Paraffin sections were deparaffinized and demelanized. Antigens were retrieved by boiling in pH 6 buffer (1.8 mM citric acid and 8.2 mM sodium citrate) for 20 min. After washing and

1-h blocking in 5% BSA/PBS, sections were immunostained for the proliferation marker PCNA. DAPI served as nuclear counterstain. Imaging was performed using an epifluorescence microscope (DM6000B; Leica Biosystems; 20× air objective). Acquired micrographs were manually premasked in ImageJ to exclude nontumor regions (e.g., hair follicle and epidermis) using the paint-brush tool. Premasked images were added to a custom CellProfiler pipeline. In short, nuclei were enhanced in the DAPI channel using EnhanceSpeckles and subsequently identified using the IdentifyPrimaryObjects module. PCNA channel micrographs were masked with the identified $DAPI^{positive}$ nuclei, and $PCNA^{high}$ nuclei were identified using the IdentifyPrimaryObjects module on the masked images, using a custom-defined threshold excluding low PCNA intensities. The sum of the $PCNA^{high}$ nuclei number divided by the sum of the $DAPI^{positive}$ nuclei was calculated using Excel. Statistical analysis and visualization were performed using Prism 6 (GraphPad Software).

Biotinylation experiments

K14-Cre$^{wt/+}$*;Par3*$^{flox/flox}$*;HGF*$^{+}$*;Cdk4*$^{R24C/R24C}$ KCs were cultured for 3 d at HC and washed with PBS containing 0.5 mM $MgCl_2$ and 0.1 mM $CaCl_2$, followed by 30-min incubation with 1.5 mg/ml biotin (EZ-Link Sulfo-NHS-SS-Biotin; Thermo Fisher Scientific) in PBS^{++} at 4°C. Biotinylated cells were washed twice in PBS^{++} containing 100 mM glycine for 20 min at 4°C, followed by washing twice with PBS^{++} and cell lysis using RIPA buffer (150 mM NaCl, 25 mM Tris, pH7.4, 5 mM EDTA, 1% NP-40, 0.1% SDS, 10% glycerol, and 1% deoxycholate). For biotin-streptavidin pull-down, 100 µl of 50% slurry NeutrAvidin beads (Thermo Fisher Scientific) was incubated with 400 µg of protein lysates for 1 h at 4°C. The beads were washed four times with RIPA buffer, and proteins were eluted from the beads by boiling in 30 µl SDS sample buffer and further processed for immunoblotting.

Pulse-chase experiments

To assess the stability of P-cadherin protein in control and $Par3^{KO}$ KCs once at the plasma membrane, biotinylation experiments were performed as described in the previous section. After biotinylation at 4°C, cells were either directly lysed or further incubated at standard culture conditions for the indicated time points. Remaining biotinylated P-cadherin was affinity purified by biotin-streptavidin pull-down as outlined in the previous section and detected by immunoblot using PCD-1 antibody.

Quantification of protein signals in Western blot analyses

The band intensity of nonsaturated Western blot signals was determined using the ImageJ rectangular tool on original digital files of scanned Western blots. Bar diagrams show the relative protein or phosphorylation signals after normalization using loading controls. In brief, the densitometry values of Western blot signals were first corrected for loading of each sample using the densitometry values of appropriate loading controls on the same membrane. These values were subsequently normalized to those of the control group, which was set to 1.

Human melanoma gene expression database analysis

Human gene expression data of published and available datasets (GEO accession nos. GSE3819 and GSE46517; Talantov et al., 2005; Kabbarah et al., 2010) were accessed via InsilicoDB and explored using the GENE-E platform (Broad Institute). Gene expression and patient survival data of the The Cancer Genome Atlas (TCGA) Skin Cutaneous Melanoma dataset (TCGA Research Network) were accessed and downloaded using cBioPortal (Cerami et al., 2012; Gao et al., 2013). Statistical analysis was performed using Prism 6.

Statistical analysis

Prism versions 5 and 6, Rstudio, and Microsoft Excel software were used for data consolidation and statistical analysis. Measures of pooled data are represented by mean and SD or SEM, as indicated in the figure legends. Comparisons of two groups were performed with unpaired Student's *t* test or unequal variances Student's *t* test (Welch's correction). Kolmogorov-Smirnov test was used for normality testing, and for non-Gaussian datasets, Mann Whitney *U* test was performed. Comparisons of more than two groups were performed by one-way ANOVA with Tukey posthoc test. The number of independent biological replicates is stated in each figure legend. P-values are ranged as follows: *, $P < 0.05$; **, $P < 0.01$; ***, $P < 0.001$; and ****, $P < 0.0001$, as detailed in the figure legends.

Online supplementary material

Video 1 shows live-cell imaging of control KC–MC co-cultures. Video 2 shows live-cell imaging of $Par3^{KO}$ KC–MC co-cultures.

ACKNOWLEDGMENTS

We thank Kathleen J. Green and Hisham Bazzi for critically reading the manuscript. We are grateful to Ricarda Stock and Esther Engelhardt for technical assistance, to the University of Cologne animal facilities, Astrid Schauss and Christian Jüngst from the Cologne Excellence Cluster on Cellular Stress Responses in Aging-Associated Diseases (CECAD) Imaging Facility, and Peter Frommolt from the CECAD Bioinformatics facility for professional support. Moreover, we thank Walter Birchmeier, Shigeo Ohno, Glenn Merlino, and Mariano Barbacid for sharing genetically modified mouse lines. We acknowledge the Z2 project of CRC829 for providing human skin tumor samples and the Broad Institute (CellProfiler) and Till Bretschneider (Quimp11b) for excellent freeware. Further, we thank members of the Iden, Niessen, and Wickström laboratories for helpful discussions.

Work in the Iden laboratory is supported by the Excellence Initiative of the German federal and state governments (CECAD), German Research Foundation (grant nos. ID79/1-1, ID79/2-1, and CRC829/A10 to S. Iden), Stiftung Kölner Krebsforschung (Exzellenz Initiieren to S. Iden), and Center for Molecular Medicine Cologne (project A3 to S. Iden). C. Mauch, C.M. Niessen, and T. Tüting are supported by German Research Foundation grants (CRC829/B04, CRC829/A01, and CRC854/A27, respectively).

The authors declare no competing financial interests.

Author contributions: conceptualization, methodology, and validation: S. Iden, M. Mauch, and P. Jeong; investigation: M. Mescher, P. Jeong, S.K. Knapp, M. Rübsam, M. Saynisch, M. Kranen, and S. Iden; formal analysis: M. Mescher, P. Jeong, and S. Iden; resources: J. Landsberg, M. Schlaak, C. Mauch, T. Tüting, and C.M. Niessen; visualization: M. Mescher and P. Jeong; writing (original draft): S. Iden; writing (review and editing): M. Mescher, P. Jeong, C. Mauch, C.M. Niessen, and S. Iden; and supervision and funding acquisition: S. Iden.

Submitted: 26 April 2016
Revised: 2 November 2016
Accepted: 6 December 2016

REFERENCES

Bald, T., T. Quast, J. Landsberg, M. Rogava, N. Glodde, D. Lopez-Ramos, J. Kohlmeyer, S. Riesenberg, D. van den Boorn-Konijnenberg, C. Hömig-Hölzel, et al. 2014. Ultraviolet-radiation-induced inflammation promotes angiotropism and metastasis in melanoma. *Nature.* 507:109–113. http://dx.doi.org/10.1038/nature13111

Bauer, R., and A.K. Bosserhoff. 2006. Functional implication of truncated P-cadherin expression in malignant melanoma. *Exp. Mol. Pathol.* 81:224–230. http://dx.doi.org/10.1016/j.yexmp.2006.07.002

Botchkareva, N.V., M. Khlgatian, B.J. Longley, V.A. Botchkarev, and B.A. Gilchrest. 2001. SCF/c-kit signaling is required for cyclic regeneration of the hair pigmentation unit. *FASEB J.* 15:645–658. http://dx.doi.org/10.1096/fj.00-0368com

Braun, K.M., C. Niemann, U.B. Jensen, J.P. Sundberg, V. Silva-Vargas, and F.M. Watt. 2003. Manipulation of stem cell proliferation and lineage commitment: visualisation of label-retaining cells in wholemounts of mouse epidermis. *Development.* 130:5241–5255. http://dx.doi.org/10.1242/dev.00703

Campbell, K., and J. Casanova. 2015. A role for E-cadherin in ensuring cohesive migration of a heterogeneous population of non-epithelial cells. *Nat. Commun.* 6:7998. http://dx.doi.org/10.1038/ncomms8998

Carpenter, A.E., T.R. Jones, M.R. Lamprecht, C. Clarke, I.H. Kang, O. Friman, D.A. Guertin, J.H. Chang, R.A. Lindquist, J. Moffat, et al. 2006. CellProfiler: image analysis software for identifying and quantifying cell phenotypes. *Genome Biol.* 7:R100. http://dx.doi.org/10.1186/gb-2006-7-10-r100

Cavallaro, U., and E. Dejana. 2011. Adhesion molecule signalling: not always a sticky business. *Nat. Rev. Mol. Cell Biol.* 12:189–197. http://dx.doi.org/10.1038/nrm3068

Cerami, E., J. Gao, U. Dogrusoz, B.E. Gross, S.O. Sumer, B.A. Aksoy, A. Jacobsen, C.J. Byrne, M.L. Heuer, E. Larsson, et al. 2012. The cBio cancer genomics portal: an open platform for exploring multidimensional cancer genomics data. *Cancer Discov.* 2:401–404. http://dx.doi.org/10.1158/2159-8290.CD-12-0095

Chang, C.-Y., H.A. Pasolli, E.G. Giannopoulou, G. Guasch, R.M. Gronostajski, O. Elemento, and E. Fuchs. 2013. NFIB is a governor of epithelial-melanocyte stem cell behaviour in a shared niche. *Nature.* 495:98–102. http://dx.doi.org/10.1038/nature11847

Chen, A., H. Beetham, M.A. Black, R. Priya, B.J. Telford, J. Guest, G.A.R. Wiggins, T.D. Godwin, A.S. Yap, and P.J. Guilford. 2014. E-cadherin loss alters cytoskeletal organization and adhesion in non-malignant breast cells but is insufficient to induce an epithelial-mesenchymal transition. *BMC Cancer.* 14:552. http://dx.doi.org/10.1186/1471-2407-14-552

Cheung, L.W.T., P.C.K. Leung, and A.S.T. Wong. 2010. Cadherin switching and activation of p120 catenin signaling are mediators of gonadotropin-releasing hormone to promote tumor cell migration and invasion in ovarian cancer. *Oncogene.* 29:2427–2440. http://dx.doi.org/10.1038/onc.2009.523

Coleman, D.J., S. Chagani, S. Hyter, A.M. Sherman, C.V. Löhr, X. Liang, G. Ganguli-Indra, and A.K. Indra. 2015. Loss of keratinocytic RXRα combined with activated CDK4 or oncogenic NRAS generates UVB-induced melanomas via loss of p53 and PTEN in the tumor microenvironment. *Mol. Cancer Res.* 13:186–196. http://dx.doi.org/10.1158/1541-7786.MCR-14-0164

Davis, M.A., R.C. Ireton, and A.B. Reynolds. 2003. A core function for p120-catenin in cadherin turnover. *J. Cell Biol.* 163:525–534. http://dx.doi.org/10.1083/jcb.200307111

Eirew, P., A. Steif, J. Khattra, G. Ha, D. Yap, H. Farahani, K. Gelmon, S. Chia, C. Mar, A. Wan, et al. 2015. Dynamics of genomic clones in breast cancer patient xenografts at single-cell resolution. *Nature.* 518:422–426. http://dx.doi.org/10.1038/nature13952

Fitzpatrick, T.B., and A.S. Breathnach. 1963. The epidermal melanin unit system. *Dermatol. Wochenschr.* 147:481–489.

Fukunaga-Kalabis, M., G. Martinez, S.M. Telson, Z.-J. Liu, K. Balint, I. Juhasz, D.E. Elder, B. Perbal, and M. Herlyn. 2008. Downregulation of CCN3 expression as a potential mechanism for melanoma progression. *Oncogene.* 27:2552–2560. http://dx.doi.org/10.1038/sj.onc.1210896

Gaffal, E., J. Landsberg, T. Bald, A. Sporleder, J. Kohlmeyer, and T. Tüting. 2011. Neonatal UVB exposure accelerates melanoma growth and enhances distant metastases in Hgf-Cdk4(R24C) C57BL/6 mice. *Int. J. Cancer.* 129:285–294. http://dx.doi.org/10.1002/ijc.25913

Gamallo, C., G. Moreno-Bueno, D. Sarrió, F. Calero, D. Hardisson, and J. Palacios. 2001. The prognostic significance of P-cadherin in infiltrating ductal breast carcinoma. *Mod. Pathol.* 14:650–654. http://dx.doi.org/10.1038/modpathol.3880367

Gao, J., B.A. Aksoy, U. Dogrusoz, G. Dresdner, B. Gross, S.O. Sumer, Y. Sun, A. Jacobsen, R. Sinha, E. Larsson, et al. 2013. Integrative analysis of complex cancer genomics and clinical profiles using the cBioPortal. *Sci. Signal.* 6:pl1. http://dx.doi.org/10.1126/scisignal.2004088

Gödde, N.J., H.B. Pearson, L.K. Smith, and P.O. Humbert. 2014. Dissecting the role of polarity regulators in cancer through the use of mouse models. *Exp. Cell Res.* 328:249–257. http://dx.doi.org/10.1016/j.yexcr.2014.08.036

Gray-Schopfer, V.C., S.C. Cheong, H. Chong, J. Chow, T. Moss, Z.A. Abdel-Malek, R. Marais, D. Wynford-Thomas, and D.C. Bennett. 2006. Cellular senescence in naevi and immortalisation in melanoma: a role for p16? *Br. J. Cancer.* 95:496–505. http://dx.doi.org/10.1038/sj.bjc.6603283

Gray-Schopfer, V., C. Wellbrock, and R. Marais. 2007. Melanoma biology and new targeted therapy. *Nature.* 445:851–857. http://dx.doi.org/10.1038/nature05661

Haass, N.K., and M. Herlyn. 2005. Normal human melanocyte homeostasis as a paradigm for understanding melanoma. *J. Investig. Dermatol. Symp. Proc.* 10:153–163. http://dx.doi.org/10.1111/j.1087-0024.2005.200407.x

Hadjantonakis, A.-K., and V.E. Papaioannou. 2004. Dynamic in vivo imaging and cell tracking using a histone fluorescent protein fusion in mice. *BMC Biotechnol.* 4:33. http://dx.doi.org/10.1186/1472-6750-4-33

Hanahan, D., and R.A. Weinberg. 2000. The hallmarks of cancer. *Cell.* 100:57–70. http://dx.doi.org/10.1016/S0092-8674(00)81683-9

Huang, L., and S.K. Muthuswamy. 2010. Polarity protein alterations in carcinoma: a focus on emerging roles for polarity regulators. *Curr. Opin. Genet. Dev.* 20:41–50. http://dx.doi.org/10.1016/j.gde.2009.12.001

Iden, S., and J.G. Collard. 2008. Crosstalk between small GTPases and polarity proteins in cell polarization. *Nat. Rev. Mol. Cell Biol.* 9:846–859. http://dx.doi.org/10.1038/nrm2521

Iden, S., W.E. van Riel, R. Schäfer, J.-Y. Song, T. Hirose, S. Ohno, and J.G. Collard. 2012. Tumor type-dependent function of the par3 polarity protein in skin tumorigenesis. *Cancer Cell.* 22:389–403. http://dx.doi.org/10.1016/j.ccr.2012.08.004

Imai, K., S. Hirata, A. Irie, S. Senju, Y. Ikuta, K. Yokomine, M. Harao, M. Inoue, T. Tsunoda, S. Nakatsuru, et al. 2008. Identification of a novel

tumor-associated antigen, cadherin 3/P-cadherin, as a possible target for immunotherapy of pancreatic, gastric, and colorectal cancers. *Clin. Cancer Res.* 14:6487–6495. http://dx.doi.org/10.1158/1078-0432.CCR-08-1086

Indelman, M., R. Bergman, R. Lurie, G. Richard, B. Miller, D. Petronius, D. Ciubutaro, R. Leibu, and E. Sprecher. 2002. A missense mutation in CDH3, encoding P-cadherin, causes hypotrichosis with juvenile macular dystrophy. *J. Invest. Dermatol.* 119:1210–1213. http://dx.doi.org/10.1046/j.1523-1747.2002.19528.x

Ireton, R.C., M.A. Davis, J. van Hengel, D.J. Mariner, K. Barnes, M.A. Thoreson, P.Z. Anastasiadis, L. Matrisian, L.M. Bundy, L. Sealy, et al. 2002. A novel role for p120 catenin in E-cadherin function. *J. Cell Biol.* 159:465–476. http://dx.doi.org/10.1083/jcb.200205115

Kabbarah, O., C. Nogueira, B. Feng, R.M. Nazarian, M. Bosenberg, M. Wu, K.L. Scott, L.N. Kwong, Y. Xiao, C. Cordon-Cardo, et al. 2010. Integrative genome comparison of primary and metastatic melanomas. *PLoS One.* 5:e10770. http://dx.doi.org/10.1371/journal.pone.0010770

Kjaer, K.W., L. Hansen, G.C. Schwabe, A.P. Marques-de-Faria, H. Eiberg, S. Mundlos, N. Tommerup, and T. Rosenberg. 2005. Distinct CDH3 mutations cause ectodermal dysplasia, ectrodactyly, macular dystrophy (EEM syndrome). *J. Med. Genet.* 42:292–298. http://dx.doi.org/10.1136/jmg.2004.027821

Kümper, S., and A.J. Ridley. 2010. p120ctn and P-cadherin but not E-cadherin regulate cell motility and invasion of DU145 prostate cancer cells. *PLoS One.* 5:e11801. http://dx.doi.org/10.1371/journal.pone.0011801

Kuphal, S., I. Poser, C. Jobin, C. Hellerbrand, and A.K. Bosserhoff. 2004. Loss of E-cadherin leads to upregulation of NFκB activity in malignant melanoma. *Oncogene.* 23:8509–8519. http://dx.doi.org/10.1038/sj.onc.1207831

Landsberg, J., J. Kohlmeyer, M. Renn, T. Bald, M. Rogava, M. Cron, M. Fatho, V. Lennerz, T. Wölfel, M. Hölzel, and T. Tüting. 2012. Melanomas resist T-cell therapy through inflammation-induced reversible dedifferentiation. *Nature.* 490:412–416. http://dx.doi.org/10.1038/nature11538

Liu, N., Q. Yu, T.J. Liu, E.P. Gebreamlak, S.L. Wang, R.J. Zhang, J. Zhang, and Y. Niu. 2012. P-cadherin expression and basal-like subtype in breast cancers. *Med. Oncol.* 29:2606–2612. http://dx.doi.org/10.1007/s12032-012-0218-8

Macara, I.G., and S. Mili. 2008. Polarity and differential inheritance—universal attributes of life? *Cell.* 135:801–812. http://dx.doi.org/10.1016/j.cell.2008.11.006

Mandeville, J.A., B. Silva Neto, A.J. Vanni, G.L. Smith, K.M. Rieger-Christ, R. Zeheb, M. Loda, J.A. Libertino, and I.C. Summerhayes. 2008. P-cadherin as a prognostic indicator and a modulator of migratory behaviour in bladder carcinoma cells. *BJU Int.* 102:1707–1714. http://dx.doi.org/10.1111/j.1464-410X.2008.08115.x

Mescher, M., and S. Iden. 2015. Par Proteins in Tumor Formation and Progression. *In* Cell Polarity 2. K. Ebnet, editor. Springer International Publishing, Cham, Switzerland. 145–165. http://dx.doi.org/10.1007/978-3-319-14466-5_6

Michels, C., T. Buchta, W. Bloch, T. Krieg, and C.M. Niessen. 2009. Classical cadherins regulate desmosome formation. *J. Invest. Dermatol.* 129:2072–2075. http://dx.doi.org/10.1038/jid.2009.17

Miller, A.J., and M.C. Mihm Jr. 2006. Melanoma. *N. Engl. J. Med.* 355:51–65. http://dx.doi.org/10.1056/NEJMra052166

Mooi, W.J., and D.S. Peeper. 2006. Oncogene-induced cell senescence—halting on the road to cancer. *N. Engl. J. Med.* 355:1037–1046. http://dx.doi.org/10.1056/NEJMra062285

Müller-Röver, S., Y. Tokura, P. Welker, F. Furukawa, H. Wakita, M. Takigawa, and R. Paus. 1999. E- and P-cadherin expression during murine hair follicle morphogenesis and cycling. *Exp. Dermatol.* 8:237–246. http://dx.doi.org/10.1111/j.1600-0625.1999.tb00377.x

Murray, N.R., K.R. Kalari, and A.P. Fields. 2011. Protein kinase Cι expression and oncogenic signaling mechanisms in cancer. *J. Cell. Physiol.* 226:879–887. http://dx.doi.org/10.1002/jcp.22463

Muzumdar, M.D., B. Tasic, K. Miyamichi, L. Li, and L. Luo. 2007. A global double-fluorescent Cre reporter mouse. *Genesis.* 45:593–605. http://dx.doi.org/10.1002/dvg.20335

Niessen, M.T., S. Iden, and C.M. Niessen. 2012. The in vivo function of mammalian cell and tissue polarity regulators—how to shape and maintain the epidermal barrier. *J. Cell Sci.* 125:3501–3510. http://dx.doi.org/10.1242/jcs.092890

Nishimura, E.K., S.A. Jordan, H. Oshima, H. Yoshida, M. Osawa, M. Moriyama, I.J. Jackson, Y. Barrandon, Y. Miyachi, and S. Nishikawa. 2002. Dominant role of the niche in melanocyte stem-cell fate determination. *Nature.* 416:854–860. http://dx.doi.org/10.1038/416854a

Nose, A., and M. Takeichi. 1986. A novel cadherin cell adhesion molecule: its expression patterns associated with implantation and organogenesis of mouse embryos. *J. Cell Biol.* 103:2649–2658. http://dx.doi.org/10.1083/jcb.103.6.2649

Osada, M., H.L. Park, Y. Nagakawa, K. Yamashita, A. Fomenkov, M.S. Kim, G. Wu, S. Nomoto, B. Trink, and D. Sidransky. 2005. Differential recognition of response elements determines target gene specificity for p53 and p63. *Mol. Cell. Biol.* 25:6077–6089. http://dx.doi.org/10.1128/MCB.25.14.6077-6089.2005

Paredes, J., C. Stove, V. Stove, F. Milanezi, V. Van Marck, L. Derycke, M. Mareel, M. Bracke, and F. Schmitt. 2004. P-cadherin is up-regulated by the antiestrogen ICI 182,780 and promotes invasion of human breast cancer cells. *Cancer Res.* 64:8309–8317. http://dx.doi.org/10.1158/0008-5472.CAN-04-0795

Paredes, J., A. Albergaria, J.T. Oliveira, C. Jerónimo, F. Milanezi, and F.C. Schmitt. 2005. P-cadherin overexpression is an indicator of clinical outcome in invasive breast carcinomas and is associated with CDH3 promoter hypomethylation. *Clin. Cancer Res.* 11:5869–5877. http://dx.doi.org/10.1158/1078-0432.CCR-05-0059

Park, J., E. Park, S.-W. Han, S.-A. Im, T.-Y. Kim, W.-H. Kim, D.-Y. Oh, and Y.-J. Bang. 2012. Down-regulation of P-cadherin with PF-03732010 inhibits cell migration and tumor growth in gastric cancer. *Invest. New Drugs.* 30:1404–1412. http://dx.doi.org/10.1007/s10637-011-9710-9

Peralta Soler, A., K.A. Knudsen, H. Salazar, A.C. Han, and A.A. Keshgegian. 1999. P-cadherin expression in breast carcinoma indicates poor survival. *Cancer.* 86:1263–1272. http://dx.doi.org/10.1002/(SICI)1097-0142(19991001)86:7<1263::AID-CNCR23>3.0.CO;2-2

Peters, E.M.J., D.J. Tobin, N. Botchkareva, M. Maurer, and R. Paus. 2002. Migration of melanoblasts into the developing murine hair follicle is accompanied by transient c-Kit expression. *J. Histochem. Cytochem.* 50:751–766. http://dx.doi.org/10.1177/002215540205000602

Rabbani, P., M. Takeo, W. Chou, P. Myung, M. Bosenberg, L. Chin, M.M. Taketo, and M. Ito. 2011. Coordinated activation of Wnt in epithelial and melanocyte stem cells initiates pigmented hair regeneration. *Cell.* 145:941–955. http://dx.doi.org/10.1016/j.cell.2011.05.004

Radice, G.L., M.C. Ferreira-Cornwell, S.D. Robinson, H. Rayburn, L.A. Chodosh, M. Takeichi, and R.O. Hynes. 1997. Precocious mammary gland development in P-cadherin–deficient mice. *J. Cell Biol.* 139:1025–1032. http://dx.doi.org/10.1083/jcb.139.4.1025

Ribeiro, A.S., and J. Paredes. 2015. P-cadherin linking breast cancer stem cells and invasion: A promising marker to identify an "intermediate/metastable" EMT state. *Front. Oncol.* 4:371. http://dx.doi.org/10.3389/fonc.2014.00371

Ribeiro, A.S., A. Albergaria, B. Sousa, A.L. Correia, M. Bracke, R. Seruca, F.C. Schmitt, and J. Paredes. 2010. Extracellular cleavage and shedding of P-cadherin: a mechanism underlying the invasive behaviour of breast cancer cells. *Oncogene.* 29:392–402. http://dx.doi.org/10.1038/onc.2009.338

Samuelov, L., E. Sprecher, D. Tsuruta, T. Bíró, J.E. Kloepper, and R. Paus. 2012. P-cadherin regulates human hair growth and cycling via canonical Wnt signaling and transforming growth factor-β2. *J. Invest. Dermatol.* 132:2332–2341. http://dx.doi.org/10.1038/jid.2012.171

Samuelov, L., E. Sprecher, K. Sugawara, S.K. Singh, D.J. Tobin, D. Tsuruta, T. Bíró, J.E. Kloepper, and R. Paus. 2013. Topobiology of human pigmentation: P-cadherin selectively stimulates hair follicle melanogenesis. *J. Invest. Dermatol.* 133:1591–1600. http://dx.doi.org/10.1038/jid.2013.18

Schadendorf, D., D.E. Fisher, C. Garbe, J.E. Gershenwald, J.-J. Grob, A. Halpern, M. Herlyn, M.A. Marchetti, G. McArthur, A. Ribas, et al. 2015. Melanoma. *Nat Rev Dis Primers.* 1:15003. http://dx.doi.org/10.1038/nrdp.2015.3

Scott, G., A. Fricke, A. Fender, L. McClelland, and S. Jacobs. 2007. Prostaglandin E2 regulates melanocyte dendrite formation through activation of PKCζ. *Exp. Cell Res.* 313:3840–3850. http://dx.doi.org/10.1016/j.yexcr.2007.07.039

Shimomura, Y., M. Wajid, L. Shapiro, and A.M. Christiano. 2008. P-cadherin is a p63 target gene with a crucial role in the developing human limb bud and hair follicle. *Development.* 135:743–753. http://dx.doi.org/10.1242/dev.006718

Slominski, A., and R. Paus. 1993. Melanogenesis is coupled to murine anagen: toward new concepts for the role of melanocytes and the regulation of melanogenesis in hair growth. *J. Invest. Dermatol.* 101:90S–97S. http://dx.doi.org/10.1111/1523-1747.ep12362991

Sotillo, R., J.F. García, S. Ortega, J. Martin, P. Dubus, M. Barbacid, and M. Malumbres. 2001. Invasive melanoma in Cdk4-targeted mice. *Proc. Natl. Acad. Sci. USA.* 98:13312–13317. http://dx.doi.org/10.1073/pnas.241338598

Souied, E., P. Amalric, M.L. Chauvet, C. Chevallier, P. Le Hoang, A. Munnich, and J. Kaplan. 1995. Unusual association of juvenile macular dystrophy with congenital hypotrichosis: occurrence in two siblings suggesting autosomal recessive inheritance. *Ophthalmic Genet.* 16:11–15. http://dx.doi.org/10.3109/13816819509057848

Sprecher, E., R. Bergman, G. Richard, R. Lurie, S. Shalev, D. Petronius, A. Shalata, Y. Anbinder, R. Leibu, I. Perlman, et al. 2001. Hypotrichosis with juvenile macular dystrophy is caused by a mutation in CDH3, encoding P-cadherin. *Nat. Genet.* 29:134–136. http://dx.doi.org/10.1038/ng716

St Johnston, D., and J. Ahringer. 2010. Cell polarity in eggs and epithelia: parallels and diversity. *Cell.* 141:757–774. http://dx.doi.org/10.1016/j.cell.2010.05.011

Suzuki, A., and S. Ohno. 2006. The PAR-aPKC system: lessons in polarity. *J. Cell Sci.* 119:979–987. http://dx.doi.org/10.1242/jcs.02898

Takayama, H., W.J. LaRochelle, R. Sharp, T. Otsuka, P. Kriebel, M. Anver, S.A. Aaronson, and G. Merlino. 1997. Diverse tumorigenesis associated with aberrant development in mice overexpressing hepatocyte growth factor/scatter factor. *Proc. Natl. Acad. Sci. USA.* 94:701–706. http://dx.doi.org/10.1073/pnas.94.2.701

Talantov, D., A. Mazumder, J.X. Yu, T. Briggs, Y. Jiang, J. Backus, D. Atkins, and Y. Wang. 2005. Novel genes associated with malignant melanoma but not benign melanocytic lesions. *Clin. Cancer Res.* 11:7234–7242. http://dx.doi.org/10.1158/1078-0432.CCR-05-0683

Tang, A., M.S. Eller, M. Hara, M. Yaar, S. Hirohashi, and B.A. Gilchrest. 1994. E-cadherin is the major mediator of human melanocyte adhesion to keratinocytes in vitro. *J. Cell Sci.* 107:983–992.

Tanimura, S., Y. Tadokoro, K. Inomata, N.T. Binh, W. Nishie, S. Yamazaki, H. Nakauchi, Y. Tanaka, J.R. McMillan, D. Sawamura, et al. 2011. Hair follicle stem cells provide a functional niche for melanocyte stem cells. *Cell Stem Cell.* 8:177–187. http://dx.doi.org/10.1016/j.stem.2010.11.029

Taniuchi, K., H. Nakagawa, M. Hosokawa, T. Nakamura, H. Eguchi, H. Ohigashi, O. Ishikawa, T. Katagiri, and Y. Nakamura. 2005. Overexpressed P-cadherin/CDH3 promotes motility of pancreatic cancer cells by interacting with p120ctn and activating rho-family GTPases. *Cancer Res.* 65:3092–3099.

Tinkle, C.L., T. Lechler, H.A. Pasolli, and E. Fuchs. 2004. Conditional targeting of E-cadherin in skin: insights into hyperproliferative and degenerative responses. *Proc. Natl. Acad. Sci. USA.* 101:552–557. http://dx.doi.org/10.1073/pnas.0307437100

Tinkle, C.L., H.A. Pasolli, N. Stokes, and E. Fuchs. 2008. New insights into cadherin function in epidermal sheet formation and maintenance of tissue integrity. *Proc. Natl. Acad. Sci. USA.* 105:15405–15410. http://dx.doi.org/10.1073/pnas.0807374105

Tormo, D., A. Ferrer, E. Gaffal, J. Wenzel, E. Basner-Tschakarjan, J. Steitz, L.C. Heukamp, I. Gütgemann, R. Buettner, M. Malumbres, et al. 2006. Rapid growth of invasive metastatic melanoma in carcinogen-treated hepatocyte growth factor/scatter factor-transgenic mice carrying an oncogenic CDK4 mutation. *Am. J. Pathol.* 169:665–672. http://dx.doi.org/10.2353/ajpath.2006.060017

Tunggal, J.A., I. Helfrich, A. Schmitz, H. Schwarz, D. Günzel, M. Fromm, R. Kemler, T. Krieg, and C.M. Niessen. 2005. E-cadherin is essential for in vivo epidermal barrier function by regulating tight junctions. *EMBO J.* 24:1146–1156. http://dx.doi.org/10.1038/sj.emboj.7600605

Tyson, R.A., E. Zatulovskiy, R.R. Kay, and T. Bretschneider. 2014. How blebs and pseudopods cooperate during chemotaxis. *Proc. Natl. Acad. Sci. USA.* 111:11703–11708. http://dx.doi.org/10.1073/pnas.1322291111

Van Den Bossche, K., J.-M. Naeyaert, and J. Lambert. 2006. The quest for the mechanism of melanin transfer. *Traffic.* 7:769–778. http://dx.doi.org/10.1111/j.1600-0854.2006.00425.x

van Roy, F. 2014. Beyond E-cadherin: roles of other cadherin superfamily members in cancer. *Nat. Rev. Cancer.* 14:121–134. http://dx.doi.org/10.1038/nrc3647

Vestweber, D., and R. Kemler. 1985. Identification of a putative cell adhesion domain of uvomorulin. *EMBO J.* 4:3393–3398.

Wagner, R.Y., F. Luciani, M. Cario-André, A. Rubod, V. Petit, L. Benzekri, K. Ezzedine, S. Lepreux, E. Steingrimsson, A. Taieb, et al. 2015. Altered E-cadherin levels and distribution in melanocytes precede clinical manifestations of vitiligo. *J. Invest. Dermatol.* 135:1810–1819. http://dx.doi.org/10.1038/jid.2015.25

Xiao, K., D.F. Allison, K.M. Buckley, M.D. Kottke, P.A. Vincent, V. Faundez, and A.P. Kowalczyk. 2003. Cellular levels of p120 catenin function as a set point for cadherin expression levels in microvascular endothelial cells. *J. Cell Biol.* 163:535–545. http://dx.doi.org/10.1083/jcb.200306001

Xue, B., K. Krishnamurthy, D.C. Allred, and S.K. Muthuswamy. 2013. Loss of Par3 promotes breast cancer metastasis by compromising cell–cell cohesion. *Nat. Cell Biol.* 15:189–200. http://dx.doi.org/10.1038/ncb2663

Yap, A.S., C.M. Niessen, and B.M. Gumbiner. 1998. The juxtamembrane region of the cadherin cytoplasmic tail supports lateral clustering, adhesive strengthening, and interaction with p120ctn. *J. Cell Biol.* 141:779–789. http://dx.doi.org/10.1083/jcb.141.3.779

Young, R.J., K. Waldeck, C. Martin, J.H. Foo, D.P. Cameron, L. Kirby, H. Do, C. Mitchell, C. Cullinane, W. Liu, et al. 2014. Loss of CDKN2A expression is a frequent event in primary invasive melanoma and correlates with sensitivity to the CDK4/6 inhibitor PD0332991 in melanoma cell lines. *Pigment Cell Melanoma Res.* 27:590–600. http://dx.doi.org/10.1111/pcmr.12228

Zhang, C.C., Z. Yan, Q. Zhang, K. Kuszpit, K. Zasadny, M. Qiu, C.L. Painter, A. Wong, E. Kraynov, M.E. Arango, et al. 2010. PF-03732010: a fully human monoclonal antibody against P-cadherin with antitumor and antimetastatic activity. *Clin. Cancer Res.* 16:5177–5188. http://dx.doi.org/10.1158/1078-0432.CCR-10-1343